A comparison of classical and modern controller design : a case study

tu/e
Research Report
ISSN 0167-9708
Coden: TEUEDE

Eindhoven
University of Technology
Netherlands

Faculty of Electrical Engineering

A Comparison of Classical and Modern Controller Design: A Case Study

by
Martin Klompstra
Ton van den Boom
Ad Damen

EUT Report 90-E-244
ISBN 90-6144-244-3

November 1990

Eindhoven University of Technology Research Reports

EINDHOVEN UNIVERSITY OF TECHNOLOGY

Faculty of Electrical Engineering
Eindhoven The Netherlands

ISSN 0167- 9708 Coden: TEUEDE

A COMPARISON OF CLASSICAL AND MODERN CONTROLLER DESIGN:
A case study

by

Martin Klompstra
Ton van den Boom
Ad Damen

EUT Report 90-E-244
ISBN 90-6144-244-3

Eindhoven
November 1990

CIP-GEGEVENS KONINKLIJKE BIBLIOTHEEK, DEN HAAG

Klompstra, Martin

A comparison of classical and modern controller design:
a case study / by Martin Klompstra, Ton van den Boom and
Ad Damen. - Eindhoven: Eindhoven University of Technology,
Faculty of Electrical Engineering. - Fig., tab. - (EUT report,
ISSN 0167-9708; 90-E-244)
Met lit.opg., reg.
ISBN 90-6144-244-3
SISO 656.2 UDC 519.71 NUGI 832
Trefw.: regeltheorie.

A COMPARISON OF CLASSICAL AND MODERN CONTROLLER DESIGN: A CASE STUDY.

Martin Klompstra **Ton van den Boom** **Ad Damen**

Measurement & Control Group,
Faculty of Electrical Engineering,
Eindhoven University of Technology,
P.O. Box 513,
NL-5600 MB Eindhoven,
The Netherlands.

Abstract

In this report, see also [8: van den Boom, Klompstra & Damen], four different types of controllers for a SISO servo tracking process are designed and compared with each other. The dynamics of the process are globally described by a first order process cascaded with a triple integrator. Both the classical control theory (PDD & LQG) and the more recently developed H_∞/H_2-control theory are used for the design of the controllers. Care has been taken to ensure that the various designs were made independently. Special attention has been paid to the triple integrating behaviour of the process and to possible saturation of the actuator. The comparison of the controllers is done in the time-domain (e.g. tracking), as well as in the frequency-domain (e.g. robust stability). The performance of the controllers is illustrated by simulations and experiments with the process under study.

Contents

1. Introduction

In the last decade new techniques for designing controllers have been developed, which resulted in the H_∞/H_2-control theory. In order to compare these new methods with the more conventional methods, like PID-type and LQG-controllers, we have designed these four types of controllers for a SISO servo tracking process. The authenticity of each design method is guarded and cross influences are avoided as much as possible.

The PID-like compensator design is based on classical tools like Bode plot, rootlocus, step response and uses only a rough model of the process and can thus be expected to perform suboptimally, but will be robustly stable. The design needs little time.

The LQG design needs a preliminary identification procedure to obtain a model of the process, proper choices of weighting matrices for the Kalman gain and the state-feedback, while robust stability is hard to establish. Consequently more designing time is needed.

For H_∞ and H_2-controllers adequate choices for weighting filters are crucial and still problematic, though robustness is easier to analyse.

It are these kinds of advantages and drawbacks, in controller design, that we want to compare for a specific process. A description and a simplified mechanical model of the process under study, the so called ball balancing system, is presented in Section 2. While Section 3, 4 and 5 are devoted to the various controller designs. Sections 6 and 7 concern the actual comparison in the time and the frequency-domain. Finally, discussion and conclusions are given in Section 8.

2. The ball balancing system

The process which is considered here is the ball balancing system, see Fig. 2.1. It has already served a decade as pilot process for educational purposes in our laboratory. In particular this highly unstable system is suited for validating systems identification and controller design techniques. The idea behind the process is quite simple: control the position of a ball which is rolling on a rail by changing the angle of the rail. The angle of the rail can be changed by a servo-motor via a spindle. The voltage, with a range of -9 to 9 volt, which is applied to the servo-amplifier and excites the servo-motor is the input signal of the system. The output signal is the position of the ball on the rail which ranges from -0.55 until 0.55 meter taken from the middle of the rail. To measure the ball position Teledeltas resistance paper has been attached to one of the inner sides of the rail, when the ball rolls over the rail it contacts the resistance paper on one side and the rail on the other side. A voltage difference of 10 Volt is applied to the ends of the resistance paper, so that the voltage measured via the ball on the other side of the rail is a measure for the position of the ball.

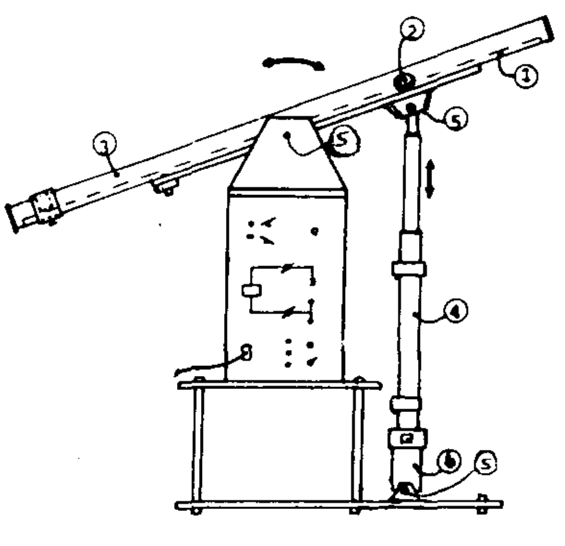

1. copper rail
2. metal ball
3. perspex tube
4. spindle
5. turn axis
6. servo motor

Fig. 2.1, the ball balancing system.

A model for the transfer function between the voltage applied to the servo-amplifier and the ball position on the rail can be derived on bases of *a priori* physical insights. Assuming that the angle of the rail is proportional to the rotation of the servo-motor-axis, the equilibrium of torques gives a relation between the voltage, the angle-acceleration and the angle-velocity:

$$\frac{d\alpha^2}{dt^2} + \Theta \frac{d\alpha}{dt} \approx K_0\, u \tag{2.1}$$

where α is the angle of the rail, Θ is the inverse time constant of the transfer from the servo-motor to the rail which can be tuned by a tachogenerator feedback, u is the control-voltage and K_0 is a constant.

The next step is to derive a relation between the acceleration of the ball and the angle of the rail. Suppose that the ball does not slip when it is rolling and neglect the centrifugal, tangential and Coriolis forces which act on the ball, then the sum of forces, as indicated by Fig. 2.2, gives:

$$m \frac{d^2y}{dt^2} \approx W - m\ g\ \sin(\alpha) \tag{2.2}$$

where m is the mass of the ball, y is the position of the ball on the rail, W is the friction force and g is the gravity acceleration.

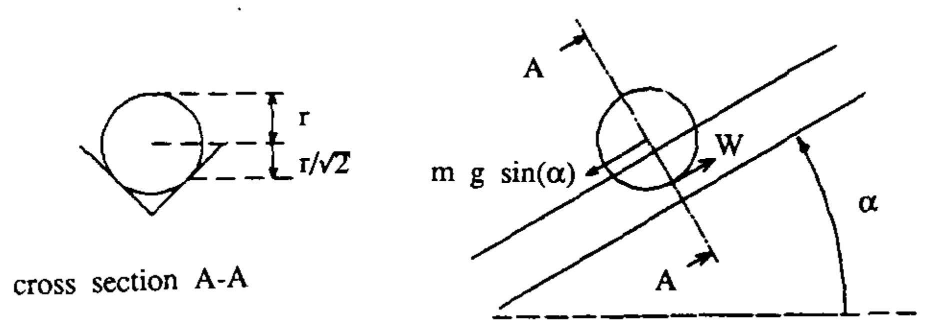

Fig. 2.2, forces acting upon the ball in the direction along the rail.

The torque $Wr/\sqrt{2}$, with r the radius of the ball see Fig. 2.2, will make the ball rotate around the axis through the center of gravity of the ball. The moment of inertia of a solid, uniform sphere with the axis through its center is $2/5mr^2$, from this follows:

$$\frac{Wr}{\sqrt{2}} = \frac{-2}{5} m r^2 \frac{d^2y}{dt^2} \frac{\sqrt{2}}{r} \quad \Rightarrow \quad W = \frac{-4}{5} m \frac{d^2y}{dt^2} \tag{2.3}$$

Substituting (2.3) into (2.2) and assuming that the angle of the rail α is kept small enough to approximate $\sin(\alpha)$ by α, then the acceleration of the ball is proportional to the angle of the rail:

$$\frac{d^2y}{dt^2} \approx \frac{-5}{9} g \alpha \tag{2.4}$$

For more details see [1: Driessen] and [9: van Bemmelen]. A linearized, approximate transfer function P(s) between servo-input U(s) in Volts and ball position Y(s) in Meters is obtained by taking the Laplace transforms of (2.1) and (2.4), substitution of the first one into the second one gives:

$$Y(s) = P(s)\, U(s)$$

where

$$P(s) = \frac{-5}{9} g \frac{K_0}{s^2 (s^2 + \ominus s)} = \frac{K}{s^3 (s + \ominus)} \tag{2.5}$$

with $K = -5/9\ g\ K_0 = -2.82\ [m/(Vs^4)]$ and $\ominus = 8.35\ [s^{-1}]$ [1].

The transfer function P(s), (2.5), can be decomposed in $P_1(s)$ and $P_2(s)$. Fig. 2.3 gives a Bode plot of P, P_1 and P_2.

$$P(s) = \frac{K}{\ominus^3} \frac{s^2 - \ominus s + \ominus^2}{s^3} - \frac{K}{\ominus^3} \frac{1}{s + \ominus} \equiv P_1(s) + P_2(s)$$

If one is only interested in frequencies up to about 1 Hz $\approx \ominus/2\pi$ Hz, then $P_1(s)$ is far dominant over $P_2(s)$, so that for these frequencies a triple integrator would be a good representation of the system. This will be used in the LQG-design.

---

1) Some of the constants given in (2.5) differ from the ones given in [1: Driessen] and [9: van Bemmelen]. The gains of the process have changed, especially the constant K_0. Therefore we have done some extra tests to tune these constants to their present values.

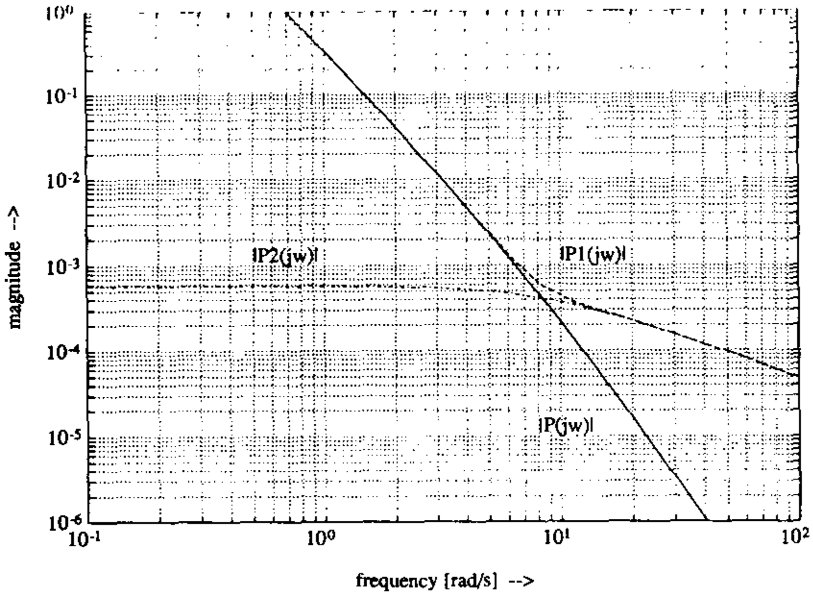

Fig. 2.3, Bode plot of decomposed transfer function of the ball balancing system.

We have chosen for doing the controller design and comparison completely in discrete-time and z-domain. The reasons for this approach are first of all that only discrete versions of the controllers can be implemented on the PC which is connected to the system, secondly that the sampling frequency of the system is only 10 Hz and finally that discrete transfer functions are easier to handle in simulations. Therefore it is necessary to have a discrete representation P(z) of (2.5). The transformation of (2.5) for zero-order- hold and sampling frequency 10 Hz yields P(z):

$$P(z) = -9.9467 \cdot 10^{-6} \, \frac{(z + 8.5156)(z + 0.8478)(z + 0.0840)}{(z - 1)^3 (z - 0.4339)} \tag{2.6}$$

The transfer function P(z), (2.6), will be used as a nominal model for the PDD, H_∞ and H_2-controller design.

In Fig. 2.4 the configuration of the system $P(z)$ with controllers $K_1(z)$ and $K_2(z)$ is given. The output, y, the actual ball position, is to track a reference signal, r. The plant input, u, is generated by passing r and y through controllers K_1 and K_2 respectively. A limiter has been built-in to bound the input signal, u, of the servo-amplifier at ±9 Volt. This limiter, since it is a non-linearity, will play an important role in the controller design.

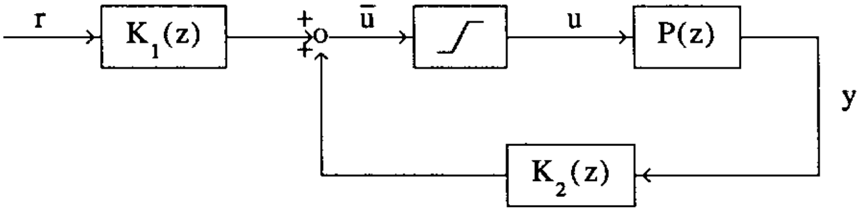

Fig. 2.4, configuration of the system and the controllers.

3. The design of the PDD-controller

The main reason for us to consider also a Proportional-Integral-Derivative (PID)-type controller in the comparison is that this is the most-implemented controller type, e.g. most industrial loops are controlled by discrete versions of the basic PID-controller.

The discrete model, (2.6), of the ball balancing system is used for the design of the PID-type controller. Note that this system has a triple integrator (3 poles in z = 1). To stabilize the system a double differentiation combined with a proportional term, hence a PDD-controller, is needed in order to get enough phase lead to compensate for the three integrators. The transfer function of a PDD-controller in the z-domain is given by:

$$K(z) = C \frac{z^2 + b_1 z + b_0}{z^2} \tag{3.1}$$

where C is the proportional term, b_1 and b_0 are constants. The two poles in $z = 0$ correspond with two poles in $s = \infty$ for the continuous-time case.

Usually a conventional-controller is implemented before the plant in the closed loop, see Fig. 3.1, instead of behind, see Fig. 2.4.

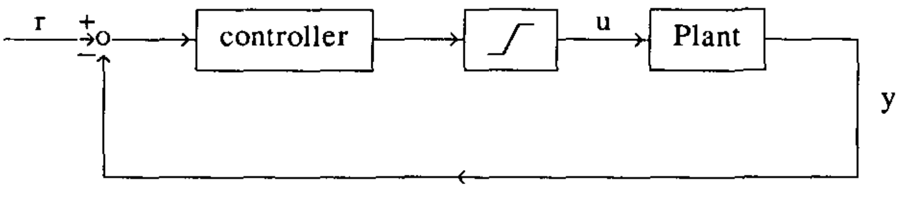

Fig. 3.1, standard closed loop configuration.

A PDD-controller has a double differentiating character so that a non-differentiative signal, i.e. a signal with discontinuities or peaks, will force the controller to produce an output signal with a very large magnitude. If the configuration of Fig. 3.1 would be used with a PDD-controller then in such a case this would result in saturation of the actuator, due to the limiter.

It is not easy to include the non-linear saturation effects in the design of the PDD-controller. Consequently, the performance of the closed-loop system can be very bad. For example Fig. 3.2 shows two tracking-simulations with the PDD-controller:

$$K(z) = -900.9310\ (z^2 - 1.9676z + 0.9686)\ /\ z^2$$

The dashed-dotted line is a simulation with the limiter and the dashed line is a simulation without the limiter. The solid line is the reference signal. This simulation shows that the discrepancy in performance can become quite big. The control voltage has peaks of 450 Volt!, while the maximum allowed input is 9 Volt. A solution would be to apply anti-windup techniques, however, this is also difficult e.g. the method described in [10: Hanus, Kinnaert & Henrotte] cannot be applied because our system does not satisfy the required conditions. This situation can be avoided by using the configuration of Fig. 2.4, where $K_2(z)$ is the PDD-controller and $K_1(z)$ is the steady state value of $(1 - K_2P)\ /\ P$ to ensure a steady state value of 1 for the transfer from r to y. This configuration has the advantage that each (non-differentiative) reference signal is not differentiated directly but is first filtered by the triple integrator of the system. This approach reduces the saturation effects considerably.

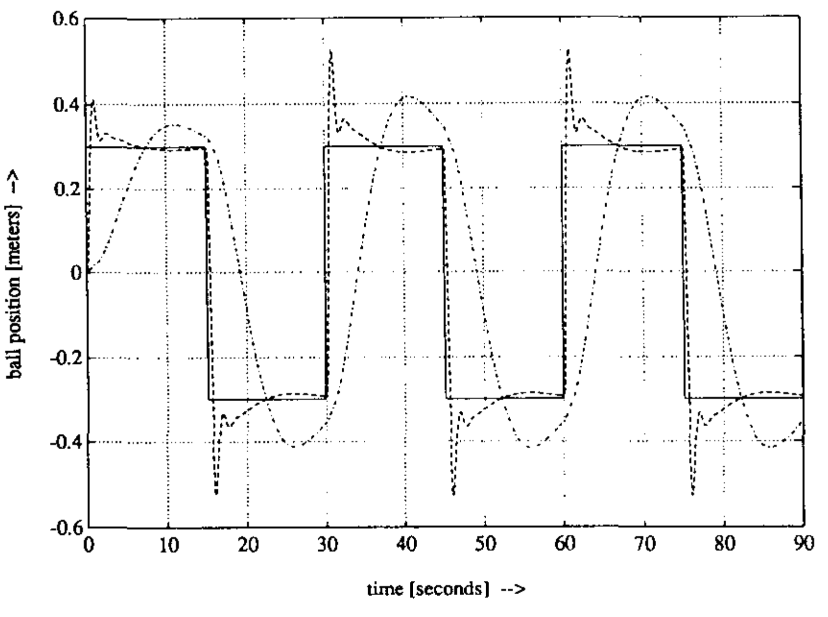

Fig. 3.2, tracking-simulation with (dash dot) and without (dashed) the limiter.

The PDD-controller has been designed as follows: choose a pair of complex conjugate zeros and tune the proportional term, (note that the designer has in fact three degrees of freedom), such that the closed loop system is internally stable (all poles inside the unit circle). Further we demand that the response to a step of 0.6 (from -0.3 to 0.3) should fulfil the following criteria:

1 - a small tracking error, measured by:

$$\sqrt{\sum_{k=0}^{N} |0.3 - y(k)|^2} \qquad \text{with N sufficiently large.}$$

2 - a small settling-time k_s, where a 2% tolerance is allowed:

$$|0.3 - y(k)| \leq 0.012 \qquad \forall\ k \geq k_S$$

3 - no saturation of the actuator.

After some trial and error with PC-MATLAB's control toolbox we obtained:

$$\left.\begin{aligned} K_1(z) &= (1 - P(1)K_2(1)) \,/\, P(1) \quad = -9.5834 \\ K_2(z) &= 933.6\ \frac{z^2 - 1.8480z + 0.8583}{z^2} \end{aligned}\right\} \tag{3.2}$$

The zeros of $K_2(z)$ are: 0.924 ± j0.067. The rootlocus is given in Fig. 6.8a-1 and a more detailed plot is given in Fig. 6.8a-2, these figures show that the closed loop poles are all inside the unit circle.

The simulated response to a step of 0.6 (from -0.3 to 0.3), see Fig. 6.1a, with PDD-controller (3.2) satisfies the criteria: The tracking error is 1.95 (with N = 150) see Table 6.1, the settling-time is about 21 samples (= 2.1 sec.) as is shown in Fig. 3.3, which is a close-up of the step response shown in Fig. 6.1a, finally Fig. 6.1b shows that there are no saturation effects.

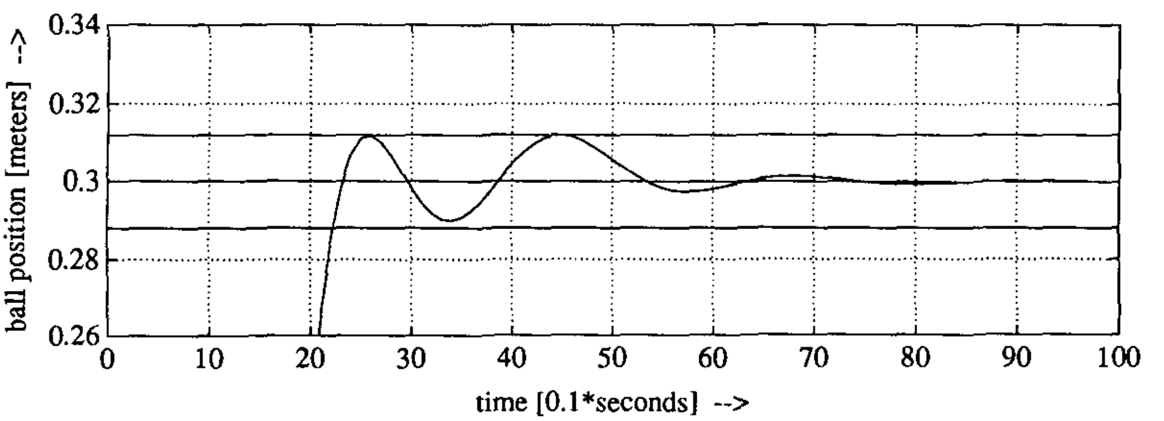

Fig. 3.3, 2% tolerance bound of the step response with the PDD-controller.

4. The design of the LQG-controller

The transfer function $P_e(z)$, (4.1), of the ball balancing system has been estimated by a prediction error method (identification toolbox in PC-MATLAB) based on input/output data, where the process was stabilized by a human operator feedback and white noise input was supplied.

$$P_e(z) = 3.2867 \cdot 10^{-4} \frac{z\ (z - 1.7392)}{(z - 1)\ (z^2 - 1.9764z + 0.979)} \tag{4.1}$$

Note that for the design of the LQG-controller a third order estimated model $P_e(z)$ is used, see also Section 2, contrary to the fourth order physical model P(z), (2.6), used for the design of the PDD, H_∞ and H_2-controller. The difference between the two models, $|P(e^{j\omega}) - P_e(e^{j\omega})|$, is plotted in Fig. 4.1. The difference is smaller than 0.1 for frequencies larger than 10^{-1} rad, but is rather large for frequencies smaller than 10^{-1} rad.

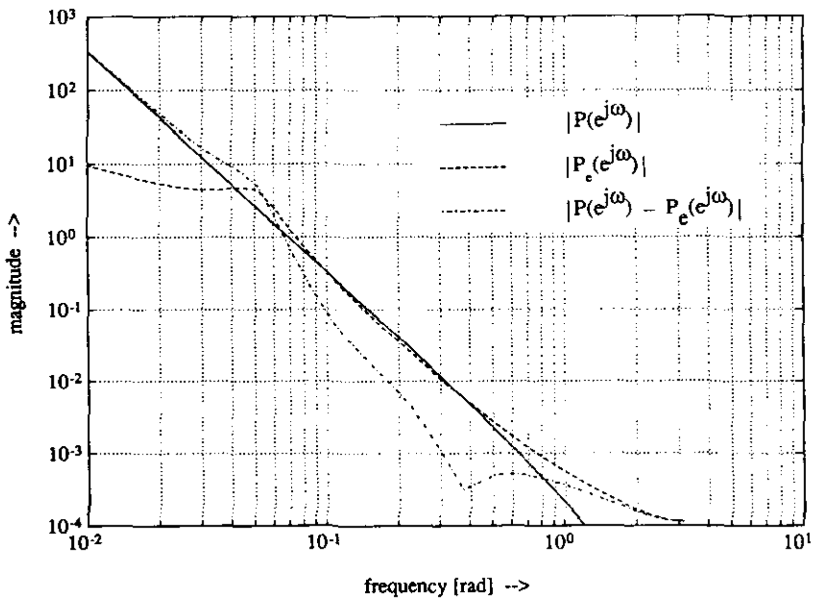

Fig. 4.1, Bode plot of P, P_e and P – P_e.

The following state space representation extended with innovations $\xi(k)$ is used:

$$\begin{aligned} x(k+1) &= Ax(k) + Bu(k) + K_G\xi(k) \\ y(k) &= Cx(k) + \xi(k) \end{aligned} \tag{4.2}$$

$$A = \begin{bmatrix} 1 & 0.1 & 0 \\ 0 & 1 & 0.1 \\ 0 & -0.026 & 0.9764 \end{bmatrix} \qquad B = \begin{bmatrix} 0 \\ 3.2867 \cdot 10^{-3} \\ -0.025 \end{bmatrix}$$

$$C = [\ 1 \quad 0.1 \quad 0\ ] \qquad K_G = \begin{bmatrix} K_1 \\ K_2 \\ K_3 \end{bmatrix} = \text{the Kalman-gains}$$

The states have been chosen such that physical meaning is apparent for proper weighting later on:

$y(k)$ = position of the ball
$x_1(k)$ = 1 sample delayed position of the ball = $y(k-1)$
$x_2(k)$ = the velocity of the ball = $(y(k) - y(k-1))/T$
$x_3(k)$ ≈ the acceleration of the ball

The Kalman-gains are tuned such that the estimated covariance, $\hat{\xi}(k)$, is close to a Dirac function [1: Driessen], resulting in:

$$K_G = [\ 1.0 \quad 9.064 \quad 2.9552\ ]^T$$

The poles of the state-observer are equal to the eigenvalues of the matrix $(A - K_G C)$ and for this choice of K_G they become:

$$p_1 = 0.938 \qquad p_2 = 0.132 \qquad p_3 = 0$$

In order to calculate the linear state feedback matrix L, see Fig. 4.2, the following quadratic cost function is minimized:

$$\sum_{k=0}^{\infty} (x^T(k)Qx(k) + u(k)Ru(k))$$

where Q and R are positive definite matrices and represent the weighting on the states and the input signal respectively. The physical meaning of this minimization is to restrict the (weighted) energy of the states while limiting the (weighted) input energy. This problem is solved by finding the unique non-negative definite symmetric solution of the associated discrete algebraic Riccati equation:

$$P = A^TPA + Q - A^TPB[R + B^TPB]^{-1}B^TPA$$

The optimal state feedback matrix then is given by:

$$L = [R + B^TPB]^{-1}B^TPA$$

After entering several Q and R matrices and simulating the step response with the corresponding state feedback, a satisfying choice for the weight factors seems:

$$Q = \begin{bmatrix} 400 & 0 & 0 \\ 0 & 250 & 0 \\ 0 & 0 & 1 \end{bmatrix} \qquad R = [\ 1.0962\ ]$$

The Q matrix implies that there is only a large weighting on the ball position and the ball velocity. The weighting factor R has been tuned in such a way that the control voltage does not cause saturation of the actuator for a blockwave with amplitude 0.3 m as reference signal. The corresponding state feedback matrix L becomes then:

$$L = [\ -15.996 \quad -27.036 \quad -17.556\ ]$$

Fig. 4.2 shows the implementation of the LQG-controller. The limiter has been implemented as part of the LQG-controller, to ensure (also in case of saturation) that the input of the observer is the same as the input of the real process. The control signal is calculated as follows:

$$\bar{u}(k) = -L[\ \{\hat{x}_1(k) - r(k)\} \quad \hat{x}_2(k) \quad \hat{x}_3(k)\ ]^T$$

The reference signal is subtracted from the first element of the state estimation, so that the difference between the actual (one sample delayed) ball-position and the desired ball-position is regulated to zero.

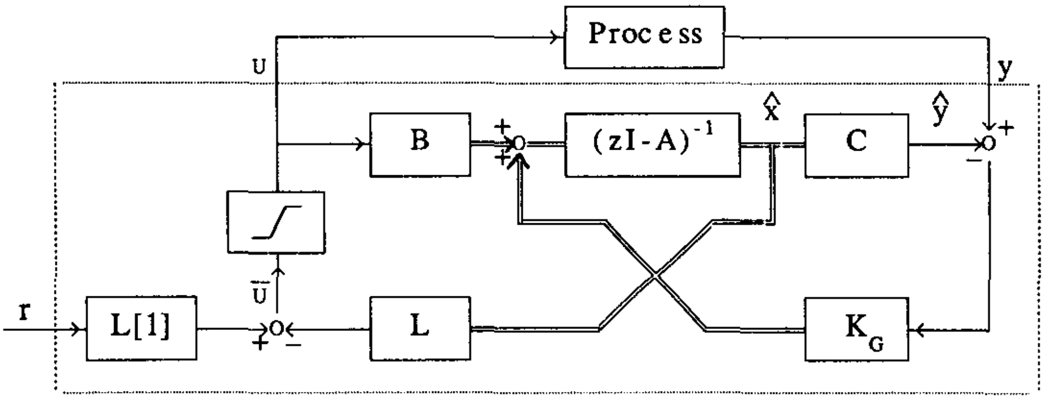

Fig. 4.2, the process with LQG-controller.

For the comparison, later on, in the frequency-domain it is useful to have a relation between the state-space configuration of Fig. 4.2 and the frequency-domain configuration of Fig. 2.4. In general, this is not possible because the limiter is part of the state-space LQG-controller implementation, i.e. for an exact frequency-domain description three transfer functions $[r\ y\ u] \longrightarrow \bar{u}$ are needed. The controller of Fig. 2.4 has only two transfer functions $[r\ y] \longrightarrow \bar{u}$. One of the design requirements for the LQG-controller was that it should not cause saturation of the actuator. This makes it possible, for this particular controller, to ignore the limiter, because $u = \bar{u}$, and to give a frequency domain description by means of two transfer functions $[r\ y] \longrightarrow \bar{u}$:

$$\hat{x}(k+1) = A\hat{x}(k) + K_G(y(k) - \hat{y}(k)) + Bu(k) =$$

$$= A\hat{x}(k) - K_G C\hat{x}(k) - BL\hat{x}(k) + BL[1]r(k) + K_G y(k)$$

Define $\mathcal{A} \equiv A - K_G C - BL$ then:

$$\Rightarrow \left.\begin{array}{l} \hat{x}(k) = (zI - \mathcal{A})^{-1}BL[1]r(k) + (zI - \mathcal{A})^{-1}K_G y(k) \\ u(k) = -L\hat{x}(k) + L[1]r(k) \end{array}\right\} \Rightarrow$$

$$u(k) = \left[-L(zI - \mathcal{A})^{-1}BL[1] + L[1]\right]r(k) + -L(zI - \mathcal{A})^{-1}K_G y(k)$$

Thus in the notation of Fig. 2.4:

$$K_1(z) \equiv \left[-L(zI - \mathcal{A})^{-1}BL[1] + L[1]\right] =$$

$$= \frac{-15.9960z^2 + 17.1157z - 1.9762}{z^2 - 0.7187z + 0.2554}$$

and

$$K_2(z) \equiv -L(zI - \mathcal{A})^{-1}K_G = \frac{312.9318z^2 - 601.3517z + 289.2763}{z^3 - 0.7187z^2 + 0.2554z}$$

5. The design of the H_∞ and H_2-controllers

This chapter considers the design of controllers for the ball-balancing system, which minimize the H_∞ or H_2-norm of a cost-criterion $\mathcal{M}$ (for a preliminary study see [2: van den Boom]). The H_∞ and H_2-norm are defined as:

$$\|H(z)\|_\infty \equiv \max_{\omega} \bar{\sigma}\left\{H(e^{j\omega})\right\}$$

$$\|H(z)\|_2 \equiv \left[\frac{1}{2\pi}\int_{-\pi}^{\pi} \mathrm{trace}\left\{H(e^{j\omega})H^*(e^{j\omega})\right\}d\omega\right]^{1/2} = \left[\sum_{k=-\infty}^{\infty} \mathrm{trace}\left\{h_t(k)h_t^*(k)\right\}\right]^{1/2}$$

with $\bar{\sigma}$ the largest singular value, '$*$' the complex conjugate transpose and $h_t(k)$ the corresponding time-domain function. We want to design a stabilizing two-degree-of-freedom controller $K(z) = [\ K_1(z)\ K_2(z)\ ]$, see Fig. 5.1, that meets tracking-performance and robustness requirements but also avoids saturation of the control-input u.

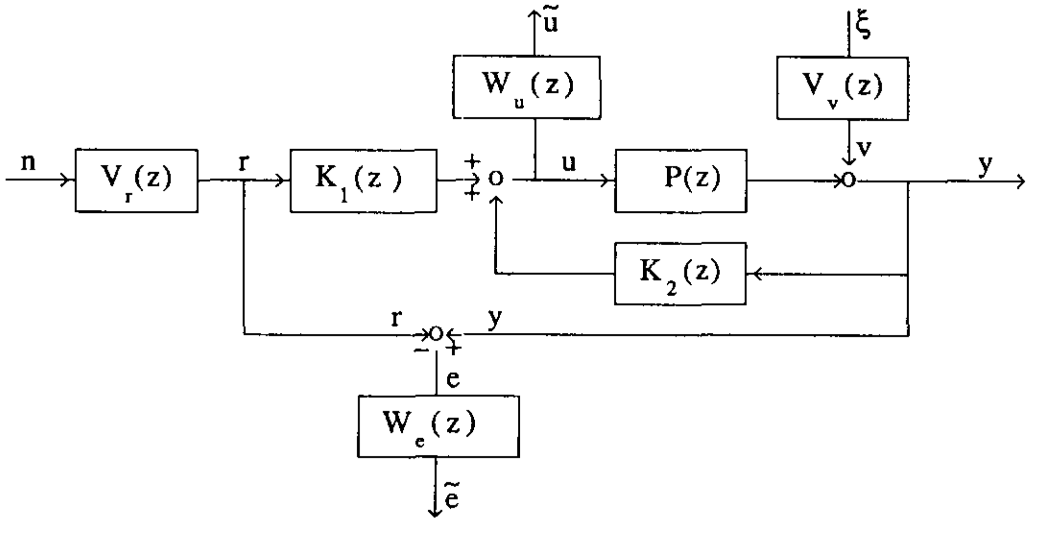

Fig. 5.1, scheme of the process with controller and weighting filters.

The reference signal r is defined as an element of the signal-class:

$$\{\ r\ |\ r = V_r n,\ \ \|n\|_2 \leq 1,\ \ V_r \in RH_\infty\ \} \tag{5.1}$$

where the weighting filter V_r describes the frequency-characteristic of the reference signal.

The first requirement is to obtain a good tracking. This is realized by minimizing the <u>weighted signal tracking error</u> of our system that is defined as:

$$\tilde{e} = W_e e = W_e(y - r) = W_e[P(1 - K_2P)^{-1}K_1 - 1]V_r n \equiv W_e E V_r n$$

with weighting filter W_e we can emphasize some frequency-band of interest. If n is chosen as the worst-case signal, then minimization of the weighted signal tracking error is equal to:

$$\boxed{\min_K \|W_e E V_r\|_\infty} \quad \text{Tracking performance measure } \left(\frac{\tilde{e}}{n}\right) \qquad (5.2)$$

with $K(z) = [\ K_1(z)\ K_2(z)\ ]$.

The second requirement is on the control signal u, which should not saturate the actuator. The class of reference signals as defined before, should only cause a control signal u in the range between -9 and +9 Volt. This is a time-constraint and has to be translated into a frequency-constraint. The control signal u can be written as:

$$u = (I - K_2P)^{-1}K_1V_r n \equiv FV_r n$$

where F is called the <u>power transfer function</u>. Define $H(z) \equiv F(z)V_r(z)$ with the corresponding time-domain function:

$$h_t(k) = \begin{cases} 0 & \text{for} \quad k < 0 \\ \dfrac{1}{2\pi}\displaystyle\int_{-\pi}^{\pi} H(e^{j\omega k})e^{j\omega k}d\omega & \text{for} \quad k \geq 0 \end{cases}$$

Let $n_t(k)$ denote the time-domain function of signal n(z):

$$n_t(k) = \frac{1}{2\pi}\int_{-\pi}^{\pi} n(e^{j\omega k})e^{j\omega k}d\omega$$

Then the time-function u(k) can be written as a convolution:

$$u(k) = \sum_{i=-\infty}^{\infty} h_t(k-i)n_t(i)$$

so

$$|u(k)| = |\sum_{i=-\infty}^{\infty} h_t(k-i)n_t(i)| \leq \left[\sum_{i=-\infty}^{\infty} |h_t(k-i)|^2\right]^{1/2}\left[\sum_{i=-\infty}^{\infty} |n_t(i)|^2\right]^{1/2} =$$

$$= \|h_t\|_2\ \|n_t\|_2 \leq \|H(z)\|_2$$

The first inequality is due to Cauchy-Schwarz, the second follows from (5.1) and Parseval's formula. A result from [7: Kung & Lin] gives the following inequality for transfer functions in the discrete-time-domain:

$$\|H(z)\|_2 \leq \|H(z)\|_\infty$$

To make sure that $|u(k)| \leq 9$ a sufficient condition is:

$$\|H(z)\|_\infty = \|F(z)V_r(z)\|_\infty \leq 9$$

This constraint is very conservative, but it can be attenuated by introducing a weighting function W_u (which will be commented upon later):

$$\boxed{\|W_u F V_r\|_\infty \leq 9} \qquad \text{Saturation constraint } \left(\frac{\tilde{u}}{n}\right) \qquad (5.3)$$

The third aim is to design a robust controller. Robust control design theories which use additive or multiplicative plant uncertainties require that the perturbed plant $\tilde{P}$ and the nominal model P should have an equal number of unstable poles and the nominal model should not contain any poles on the unit-circle (in the continuous-time case: jω-axis poles). Our nominal plant model P(z), however, has three poles in z = 1. Therefore we will not consider additive or multiplicative plant uncertainties. A good alternative expression for plant uncertainties, especially in this case, is stable-factor perturbations, i.e perturbations on the left coprime factors of the nominal plant, see [6: Vidyasagar & Kimura]. The idea is shown in Fig. 5.2.

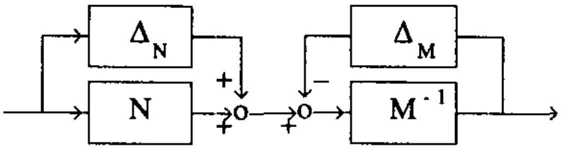

Fig. 5.2, stable-factor perturbation.

An appealing interpretation of stable-factor perturbations can be given by considering a plant which is factorized in its unstable and stable part. Suppose, the nominal model P is factorized as:

$$P = P_{unstable} P_{stable} = M^{-1}N$$

with M^{-1} unstable (but M stable!) and N stable. Let Δ_M be the stable model-error on the inverse of the unstable part M^{-1}:

$$\tilde{P}^{-1}_{unstable} = M + \Delta_M$$

and Δ_N the stable model-error on the stable part N:

$$\tilde{P}_{stable} = N + \Delta_N$$

Hence the perturbed plant $\tilde{P}$ becomes:

$$\tilde{P} = \tilde{P}_{unstable}\tilde{P}_{stable} = (M + \Delta_M)^{-1}(N + \Delta_N)$$

which is the configuration of Fig. 5.2. This factorization approach can be stated more formally by means of left coprime factorization. A robustness constraint can then be given by considering H_∞-norm bounds of perturbations on the coprime factors. Let M, N $\in RH_\infty$ be a left coprime factorization of the nominal plant model $P = M^{-1}N$. Take as plant uncertainties additive stable perturbations Δ_M and Δ_N of these coprime factors such that $(M + \Delta_M)$ and $(N + \Delta_N)$ form a left coprime factorization of the perturbed plant $\tilde{P}$, see Fig. 5.2:

$$\tilde{P} = (M + \Delta_M)^{-1}(N + \Delta_N)$$

The following theorem is from [5: McFarlane (remark 3.11 with $W = \begin{bmatrix} W_M & 0 \\ 0 & W_N \end{bmatrix}$)].

Theorem:

The controller K stabilizes $\tilde{P} = (M + \Delta_M)^{-1}(N + \Delta_N)$ for all perturbations $[\ \Delta_M\ \Delta_N\ ]$ satisfying:

$$\| [\ \Delta_M W_M^{-1} \quad \Delta_N W_N^{-1}\ ] \|_\infty < \varepsilon \qquad W_N,\ W_N^{-1},\ W_M,\ W_M^{-1} \in RH_\infty \quad (5.4)$$

(W_N and W_M are thus known weighting functions)

if and only if

(1) K stabilizes the nominal plant P

(2) $$\left\| \begin{bmatrix} W_M(I - PK)^{-1}M^{-1} \\ W_N K\ (I - PK)^{-1}M^{-1} \end{bmatrix} \right\|_\infty \le \varepsilon^{-1}$$

∎

Note that the above theorem puts no restriction on the nominal and perturbed plant's unstable poles. The poles in z = 1 of our nominal model P(z) (which become zeros of M) may be perturbed in such a way that they run into or out of the unit-circle, as long as condition (5.4) is satisfied.

So the optimization of the plant's robustness subjected to stable-factor perturbations is equal to:

$$\boxed{\min_{K} \left\| \begin{bmatrix} W_M(I - PK_2)^{-1}M^{-1} \\ W_N K_2(I - PK_2)^{-1}M^{-1} \end{bmatrix} \right\|_\infty}$$

with $K(z) = [\ K_1(z)\ K_2(z)\ ]$. Note that the robustness of the controller $K(z)$ depends only on the controller $K_2(z)$. In Fig. 5.1 it is easily seen that when $V_v = M^{-1}$, $W_u = W_N$, $W_e = W_M$ and ξ is a signal in the class $\|\xi\|_2 \le 1$ the optimization of the plant's robustness subjected to stable-factor perturbations is equal to:

$$\boxed{\min_{K} \left\| \begin{bmatrix} W_e(I - PK_2)^{-1}V_v \\ W_u K_2(I - PK_2)^{-1}V_v \end{bmatrix} \right\|_\infty} \quad \text{Robustness} \left(\begin{bmatrix} \tilde{e}/\xi \\ \tilde{u}/\xi \end{bmatrix} \right) \tag{5.5}$$

with $K(z) = [\ K_1(z)\ K_2(z)\ ]$. Of course we lose some degrees of freedom by this choice of W_M and W_N, but solving the problem will become much easier.

Writing the problem as a standard problem

The final criterion, which optimizes all mentioned requirements (tracking performance, saturation constraint and robustness) can be formulated as a standard problem, see [4: Francis]. The transfer functions from the input signals n, ξ and the control signal u to the regulated outputs $\tilde{e}$, $\tilde{u}$ and the controller-input signals r, y can be written in matrix-notation by combining (5.2), (5.3) and (5.5):

$$\begin{bmatrix} \tilde{e} \\ \tilde{u} \\ \hline r \\ y \end{bmatrix} = \begin{bmatrix} W_e(y-r) \\ W_u u \\ \hline r \\ y \end{bmatrix} = \left[\begin{array}{cc|c} -W_eV_r & W_eV_v & W_eP \\ 0 & 0 & W_u \\ \hline V_r & 0 & 0 \\ 0 & V_v & P \end{array}\right] \begin{bmatrix} n \\ \xi \\ \hline u \end{bmatrix}$$

with

$$u = [\ K_1 \quad K_2\ ] \begin{bmatrix} r \\ y \end{bmatrix}$$

Now define:

$$\left[\begin{array}{c|c} G_{11} & G_{12} \\ \hline G_{21} & G_{22} \end{array}\right] \equiv \left[\begin{array}{cc|c} -W_eV_r & W_eV_v & W_eP \\ 0 & 0 & W_u \\ \hline V_r & 0 & 0 \\ 0 & V_v & P \end{array}\right]$$

The criterion becomes:

$$\min_K \|\mathcal{M}(K)\|_\infty = \min_K \|G_{11} + G_{12}K(I - G_{22}K)^{-1}G_{21}\|_\infty =$$

$$= \min_K \left\| \begin{bmatrix} W_eEV_r & W_e(I - PK_2)^{-1}V_v \\ W_uFV_r & W_uK_2(I - PK_2)^{-1}V_v \end{bmatrix} \right\|_\infty$$

$$= \min_K \left\| \begin{bmatrix} W_e[P(I - K_2P)^{-1}K_1 - I]V_r & W_e(I - PK_2)^{-1}V_v \\ W_u(I - K_2P)^{-1}K_1V_r & W_uK_2(I - PK_2)^{-1}V_v \end{bmatrix} \right\|_\infty \tag{5.6}$$

with $K(z) = [\ K_1(z)\ K_2(z)\ ]$

In the case of minimizing the H_∞-norm of $\mathcal{M}$ only the worst-case signal $[\ n\ \xi\ ]^T$ is considered. As an alternative one can study a more "average" behaviour by assuming that the signal $[\ n\ \xi\ ]^T$ is unit covariance white noise and minimize the covariance of the output signal $[\ \tilde{e}\ \tilde{u}\ ]^T$. This is equivalent to minimizing the H_2-norm of $\mathcal{M}$, see [3: Doyle], thus (5.6) becomes:

$$\min_K \|\mathcal{M}(K)\|_2 = \min_K \|G_{11} + G_{12}K\ (I - G_{22}K)^{-1}G_{21}\|_2 \tag{5.7}$$

Recall that until now the complete design is done in the z-domain. To calculate the optimal controllers the final criteria (5.6) and (5.7) are transformed by means of the bilinear transformation to an equivalent continuous time version. The procedure of [11: Doyle, Glover, Khargonekar & Francis] and [3: Doyle] can then be used to compute the controllers. Finally the inverse bilinear transformation is used to get the optimal controllers in the z-domain.

Choice of the weighting-functions:

Before we can start the design procedure the weighting functions W_e, W_u, V_r and V_v have to be chosen. As mentioned above, the weighting filter V_r describes the frequency-characteristic of the reference signal r. In principle we would like to choose:

$$V_r(z) = 0.6\ \frac{z}{z - 1}$$

so that the reference signals would have the character of a step function. However, this choice of $V_r(z)$ also yields energy-unbounded signals r with $\|r\|_2 = \infty$ i.e. when $n(e^{j\omega}) \neq 0$ for $\omega = 0$. In that case minimization of criterion $\|\mathcal{M}(K)\|_\infty$ will fail. Besides there is no point in controlling the ball-position-error to less than the resolution of the measuring system.

These considerations allow the weighting filter to be leveled off at low frequencies. So we take:

$$V_r(z) = 0.6 \frac{z}{z - 0.995}$$

This corresponds with the Fourier-transform of a step-like function $v_r(k) = 0.6\ (0.995^k)$.

The next step is to calculate a left coprime factorization of the nominal model $P = M^{-1}N$. The main problem is a good choice for the poles of N and M. The poles of M are chosen the same as the poles of the LQG-observer (the eigenvalues of the matrix $A - K_G C$). The zeros of M are of course the three unstable poles of the system in $z = 1$. By this choice $V_v = M^{-1}$ describes the character of the output-disturbance (using the LQG-model) and signal $v = V_v \xi$, see Fig. 5.1, gets the character of the output-noise. The coprime-factors become:

$$N(z) = -4.7744 \cdot 10^{-7} \frac{(z + 8.5156)(z + 0.8478)(z + 0.0840)}{z(z - 0.938)(z - 0.132)(z - 0.4339)}$$

$$M(z) = 25 \frac{(z - 1)^3}{z(z - 0.938)(z - 0.132)}$$

W_e is the weighting on the signal-tracking-error and the inverse of the weighting on one of the coprime factor perturbations (Δ_M). W_e is chosen as the inverse of the desired signal-tracking-error. The signal-tracking-error should be small for low frequencies, thus the weighting on these frequencies must be large compared to the other frequencies.

$$W_e(z) = \left[0.660 \frac{(z^2 - 1.75z + 0.9025)(z - 0.999)}{(z - 0.4688)(z - 0.7072)(z - 0.9950)} \right]^{-1} =$$

$$= 1.516 \frac{(z - 0.4688)(z - 0.7072)(z - 0.9950)}{(z^2 - 1.75z + 0.9025)(z - 0.999)}$$

W_u is the weighting on the power transfer function and the inverse of the weighting on one of the coprime factor perturbations (Δ_N). The weighting filter W_u must be chosen such that the control voltage does not cause saturation of the actuator. Simulations of the response to a step of 0.6 showed that a suitable choice seems:

$$W_u(z) = 2.576 \frac{(z - 0.9)^2}{(z + 0.8)^2}$$

Bode plots of the weighting filters V_r, V_v, W_e and W_u are given in Fig. 5.3.

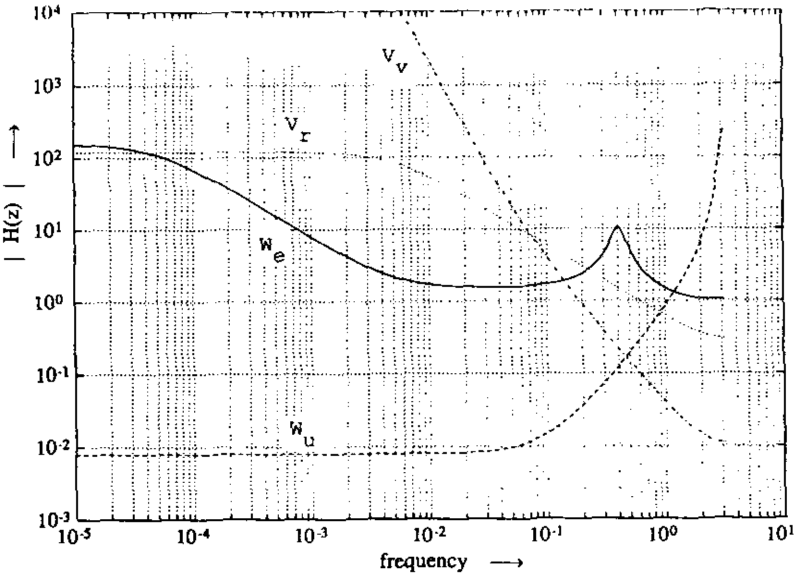

Fig. 5.3, Bode plots of the weighting-filters.

The controllers

Minimizing the criteria for this choice of weighting functions and using the design method of [11: Doyle, Glover, Khargonekar & Francis] and [3: Doyle] the following results are obtained:

$$\min_{K} \|\mathcal{M}(K)\|_\infty = 15, \text{ where the optimal controller } K_\infty(z) \text{ is equal to}$$

$$K_\infty(z) = [\, K_{1\infty}(z) \quad K_{2\infty}(z) \,], \text{ with}$$

$$K_{1\infty}(z) = -0.7606 \frac{(z+1)(z+0.8)^2(z-0.9380)(z-0.9950)(z^2-1.7738z+0.9669)(z-0.4339)}{z(z-0.99995)(z^2-1.7500z-0.9025)(z^2-1.5405z+0.8133)(z^2-0.6345z+0.1624)}$$

$$K_{2\infty}(z) = 18.34 \frac{(z+1)(z+0.8)^2(z^2-1.7609z+0.9120)(z-0.9950)(z^2-1.9111z+0.9140)(z-0.4339)}{z(z-0.99995)(z^2-1.7500z-0.9025)(z^2-1.5405z+0.8133)(z^2-0.6345z+0.1624)(z-0.1320)}$$

and

$$\min_{K} \|\mathcal{M}(K)\|_2 = 6.39, \text{ where the optimal controller } K_T(z) \text{ is equal to}$$

$$K_T(z) = [\, K_{1T}(z) \quad K_{2T}(z) \,], \text{ with}$$

$$K_{1T}(z) = -0.3758 \frac{(z+0.8)^2(z^2-1.6744z+0.8285)(z-0.9950)(z-0.9380)}{z(z-0.999)(z^2-1.7500z-0.9025)(z^2-1.7031z+0.8667)(z+0.4339)}$$

$$K_{2T}(z) = 10.04 \frac{(z+0.8)^2(z^2-1.7474z+0.9023)(z-0.9950)(z^2-1.9289z-0.9309)}{z(z-0.999)(z^2-1.7500z-0.9025)(z^2-1.7031z+0.8667)(z+0.4339)(z-0.1320)}$$

6. Comparison in the time domain

To compare such different controllers as PDD, LQG, H_∞ and H_2-optimal controllers one has to define some criteria for comparison. In this section we consider criteria in the time domain, in Section 7 we will consider criteria in the frequency domain.

In the time domain the four controllers can be compared by considering the responses y(k) and u(k) for different reference signals: A step function and a special test signal. The step function is defined as r(k) = -0.3 m for $k < 0$ and r(k) = 0.3 m for $k \geq 0$. The special test signal f(k), see Fig. 6.3, consists of a sequence of characteristic functions, respectively a set point (for $0 \leq k < 50$), a ramp function (for $50 \leq k < 150$) again a set point (for $150 \leq k < 200$), a parabolic function (for $200 \leq k < 400$), a staircase function (for $400 \leq k < 600$), a saw tooth function (for $600 \leq k < 700$), a set point (for $700 \leq k < 750$), a noise signal (for $750 \leq k < 950$) and finally a set point (for $950 \leq k < 1000$).

Measurements on the real process controlled by the implemented controllers are compared with simulations on a computer with process-model P(z) as given in (2.6).

Fig. 6.1a to 6.1h show the simulated and measured step responses and the corresponding control signals for each controller. Fig. 6.2a & 6.2b show respectively the simulated step responses and the corresponding control signals of the four controllers in one figure. The four measured step responses and the corresponding control signals are respectively shown in Fig. 6.2c & 6.2d. The general conclusion is: The PDD and the H_∞-controller perform best, but need larger impulse peaks than the LQG and the H_2-controller. Also the correspondence between simulation and actual measurements is best for the PDD and the H_∞-controller.

Fig. 6.3a to 6.3h show the simulated and measured responses and the corresponding control signals to the special test function f(k) for each controller. The performance of the PDD-controller is here significantly better than the performances of the other controllers.

Define:

The signal tracking error: $\quad STE = \sqrt{\sum_{k=0}^{150} |r(k) - y(k)|^2}$

The supplied energy: $\quad SE = \sqrt{\sum_{k=0}^{150} |u(k)|^2}$

The values of STE and SE, for all four controllers, are calculated for the simulated and the measured data and are given in Table 6.1:

	Simulation		Measurement	
	STE	SE	STE	SE
PDD	1.95	19.11	1.97	19.06
LQG	1.99	14.91	2.06	14.12
H_∞	2.10	20.13	2.19	20.45
H_2	2.36	11.84	2.75	9.65

Table 6.1, the signal tracking error and supplied energy for the four types of controllers in simulation and measurement.

From Table 6.1 follows that the PDD and the H_∞-controller use more energetic control signals in simulation as well as in the real situation, this keeps the difference between simulated and measured performance small. In this respect they are more robust.

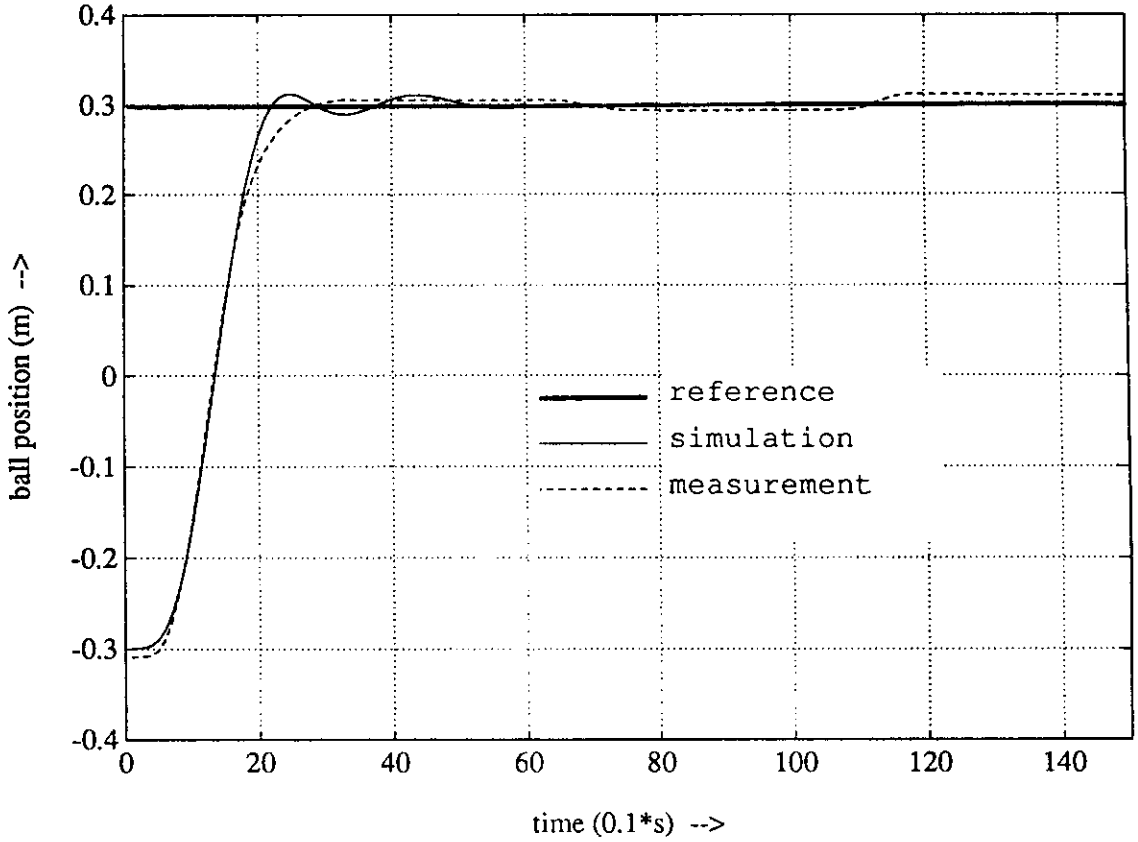

Fig. 6.1a, simulated and measured step response PDD-controller.

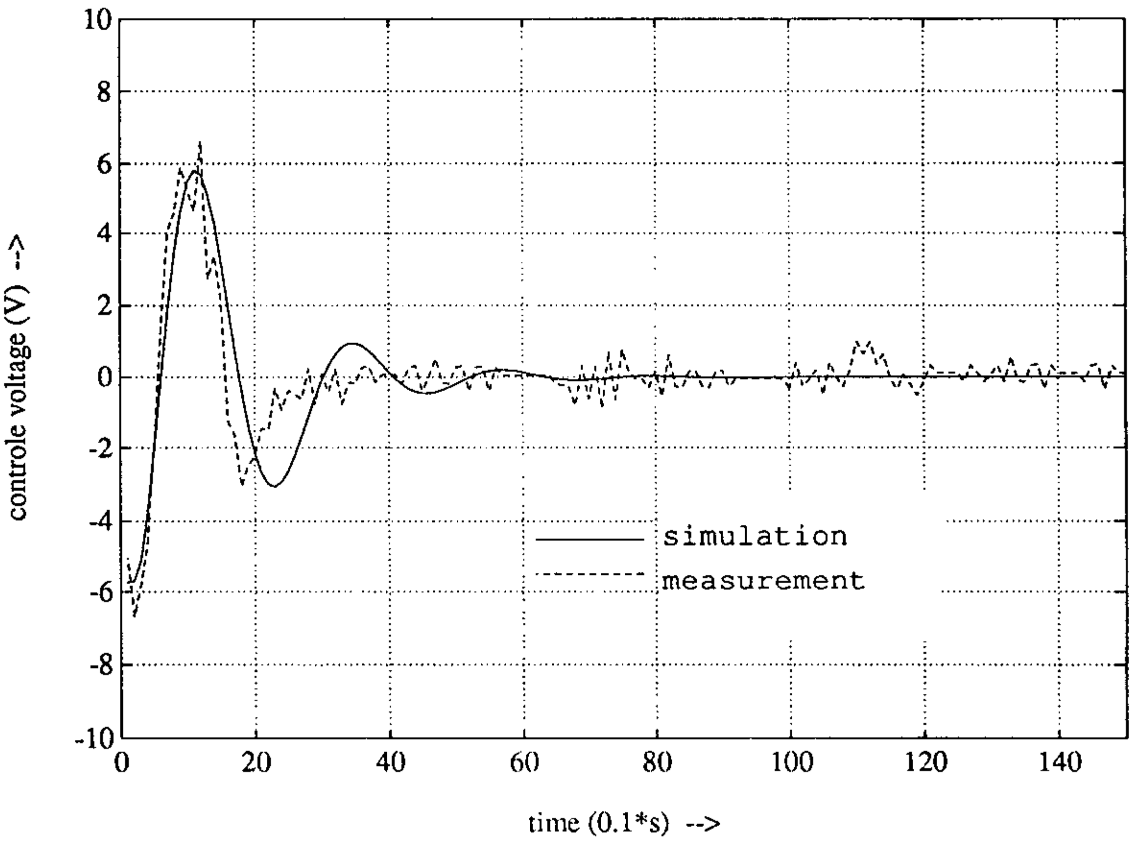

Fig. 6.1b, simulated and measured control voltage PDD-controller.

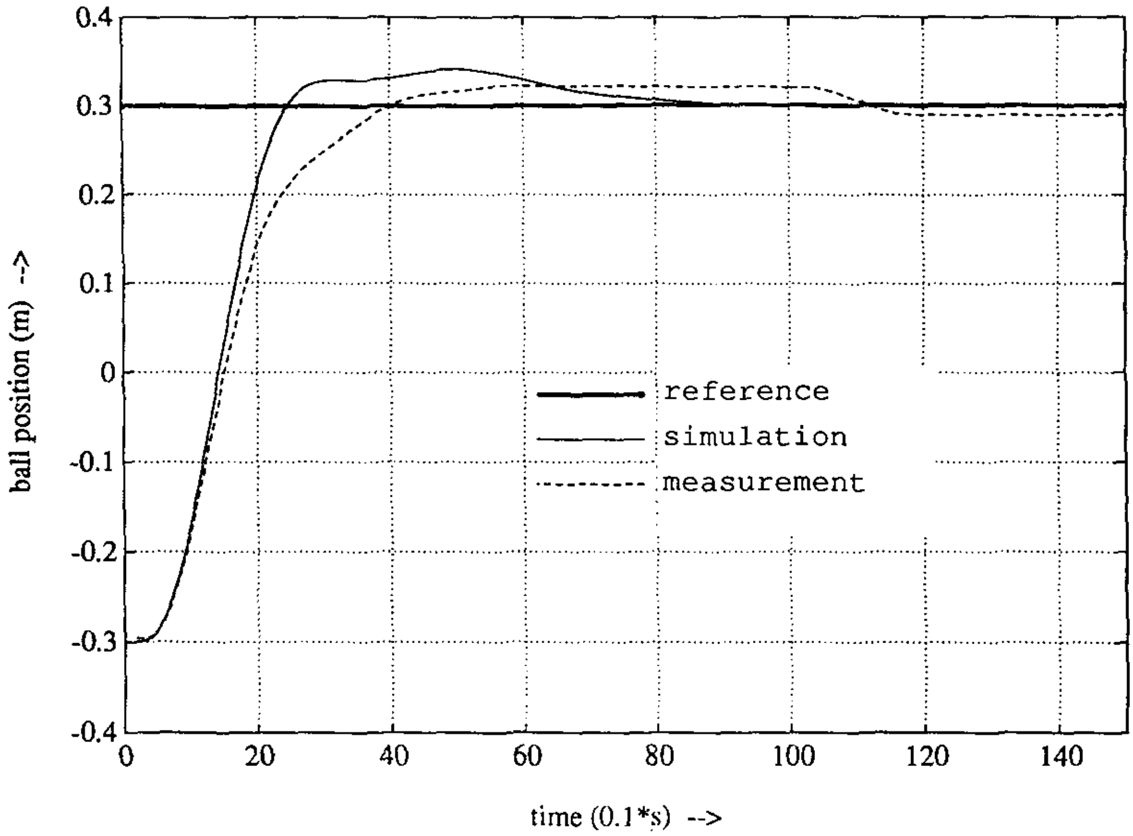

Fig. 6.1c, simulated and measured step response LQG-controller.

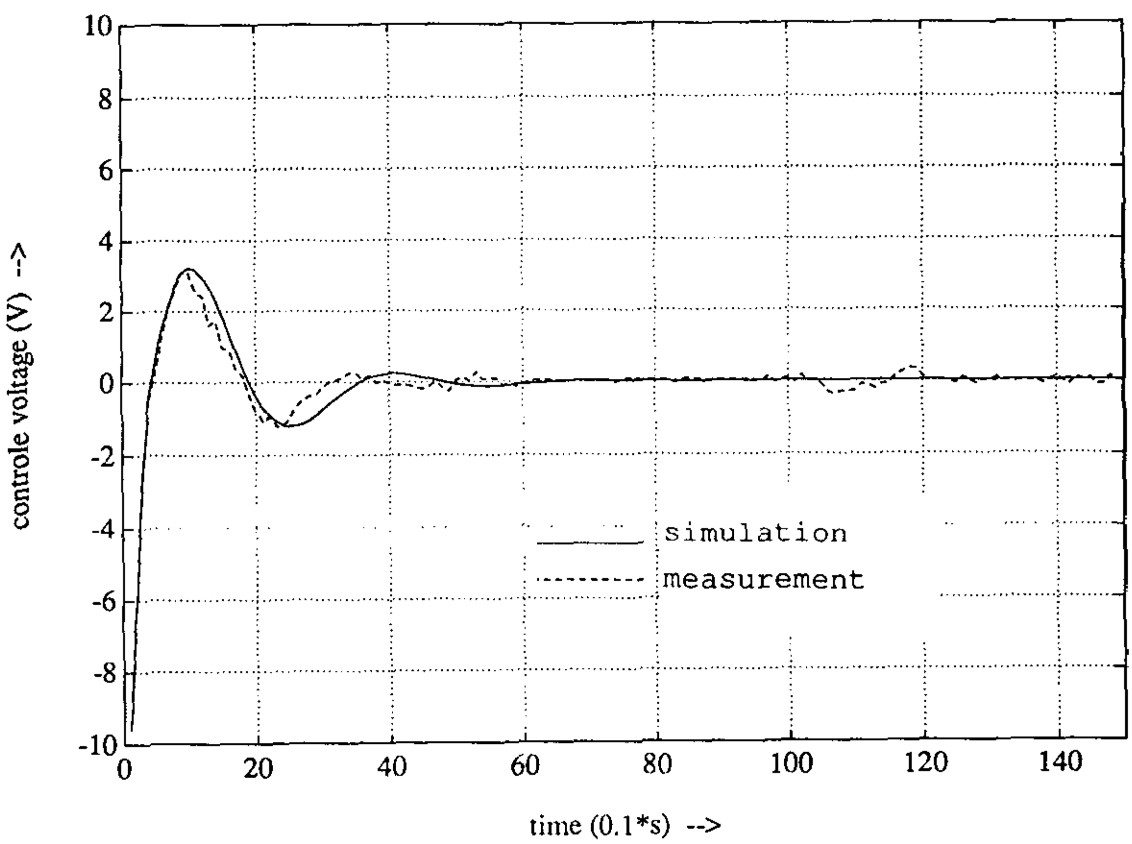

Fig. 6.1d, simulated and measured control voltage LQG-controller.

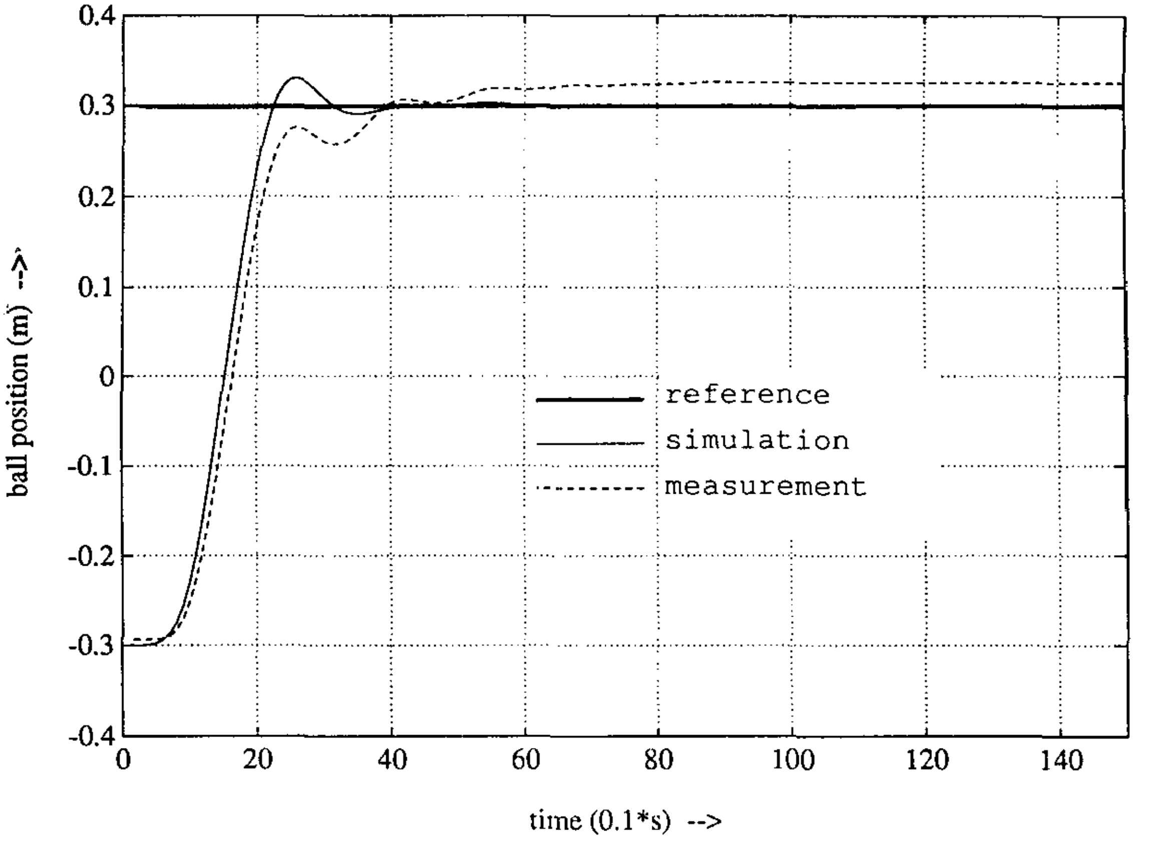

Fig. 6.1e, simulated and measured step response H_∞-controller.

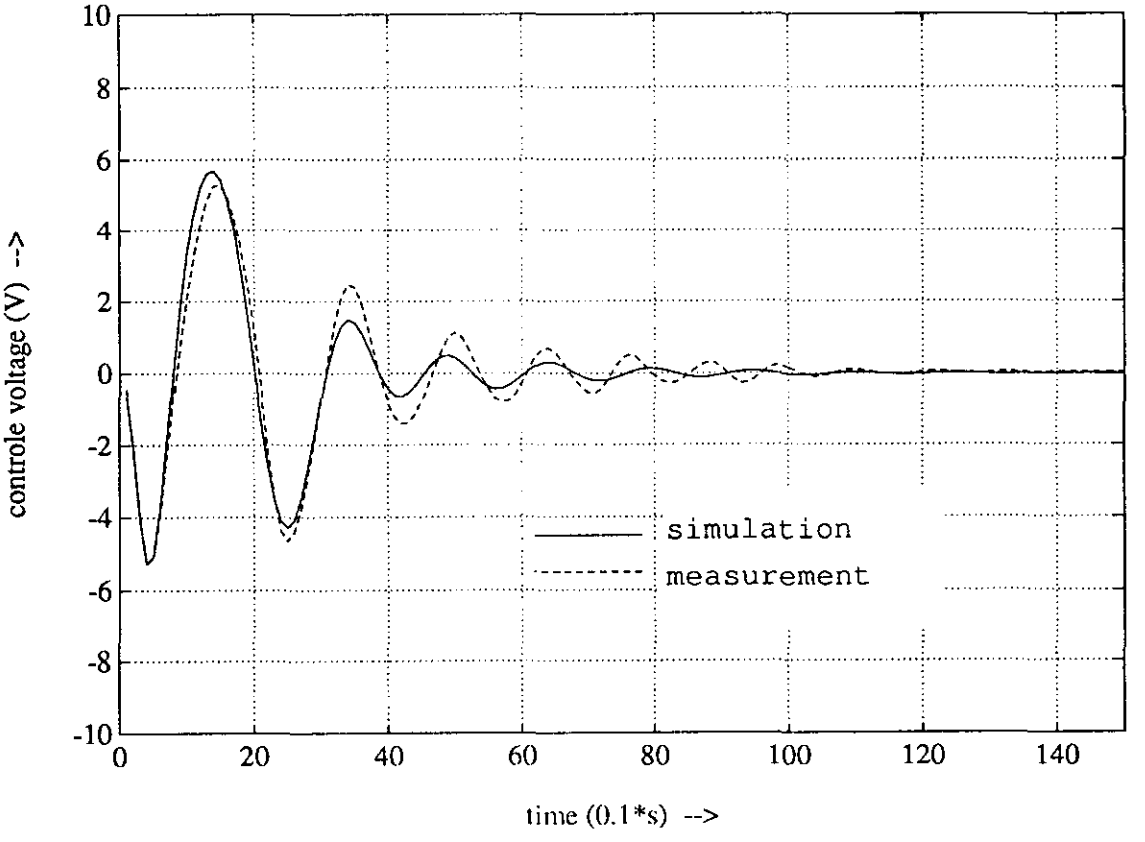

Fig. 6.1f, simulated and measured control voltage H_∞-controller.

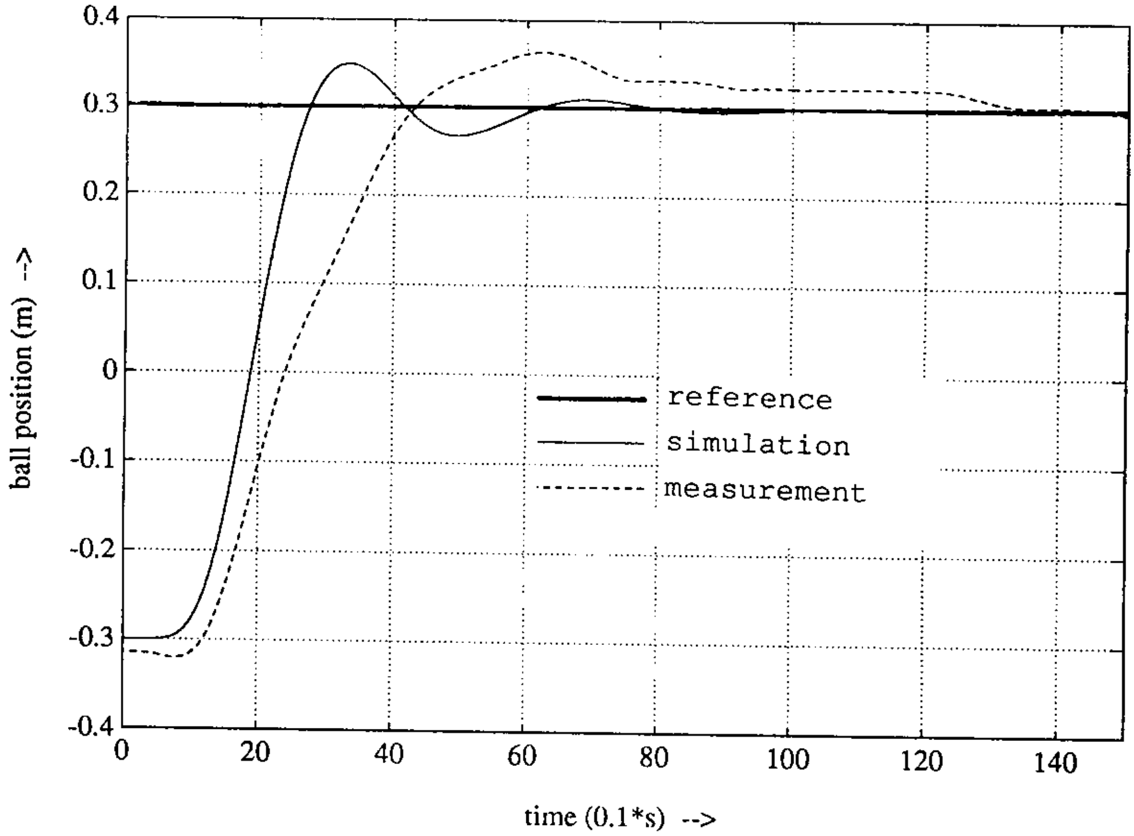

Fig. 6.1g, simulated and measured step response H_2-controller.

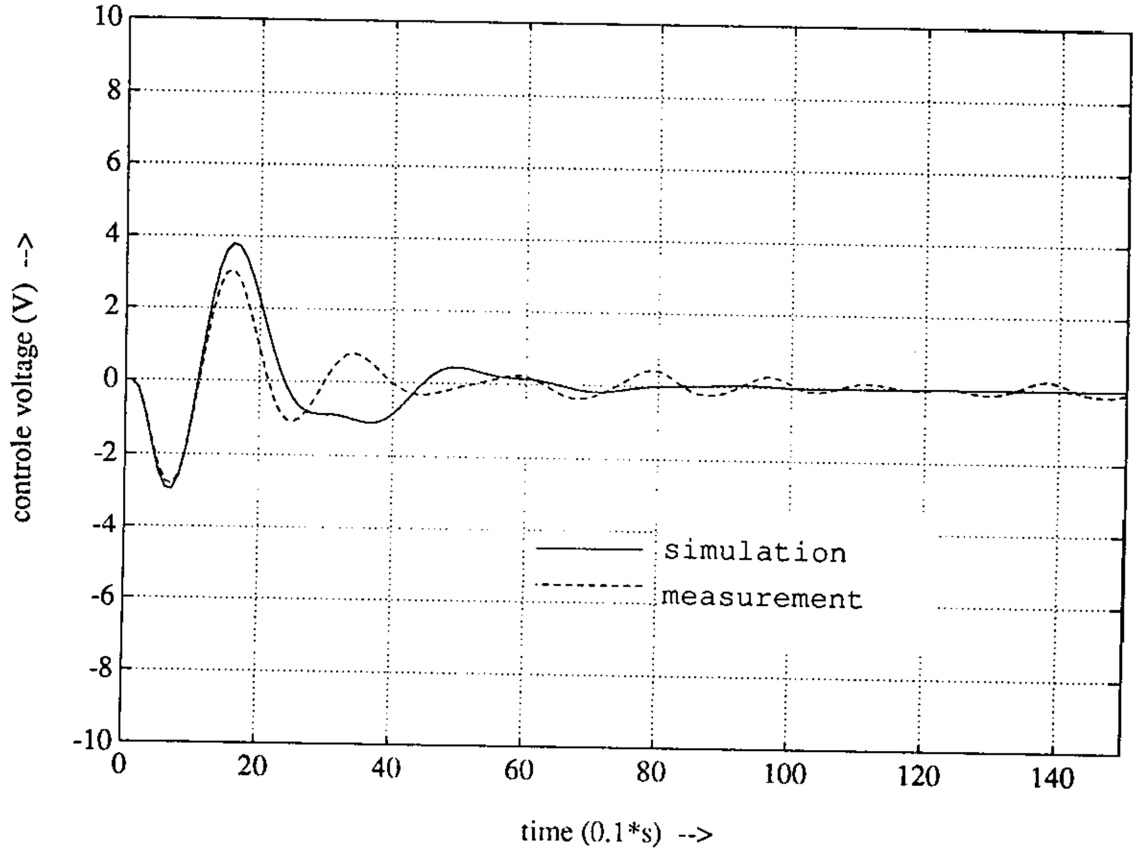

Fig. 6.1h, simulated and measured control voltage H_2-controller.

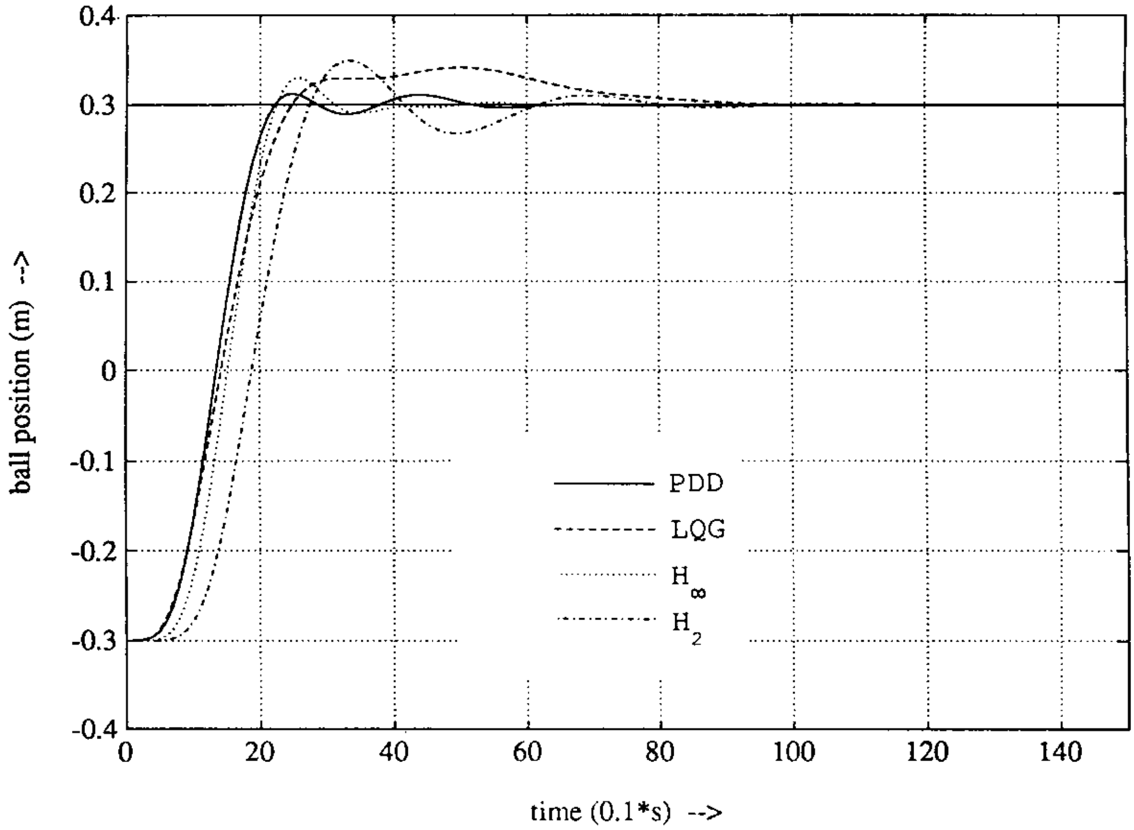

Fig. 6.2a, simulated step responses of all four controllers.

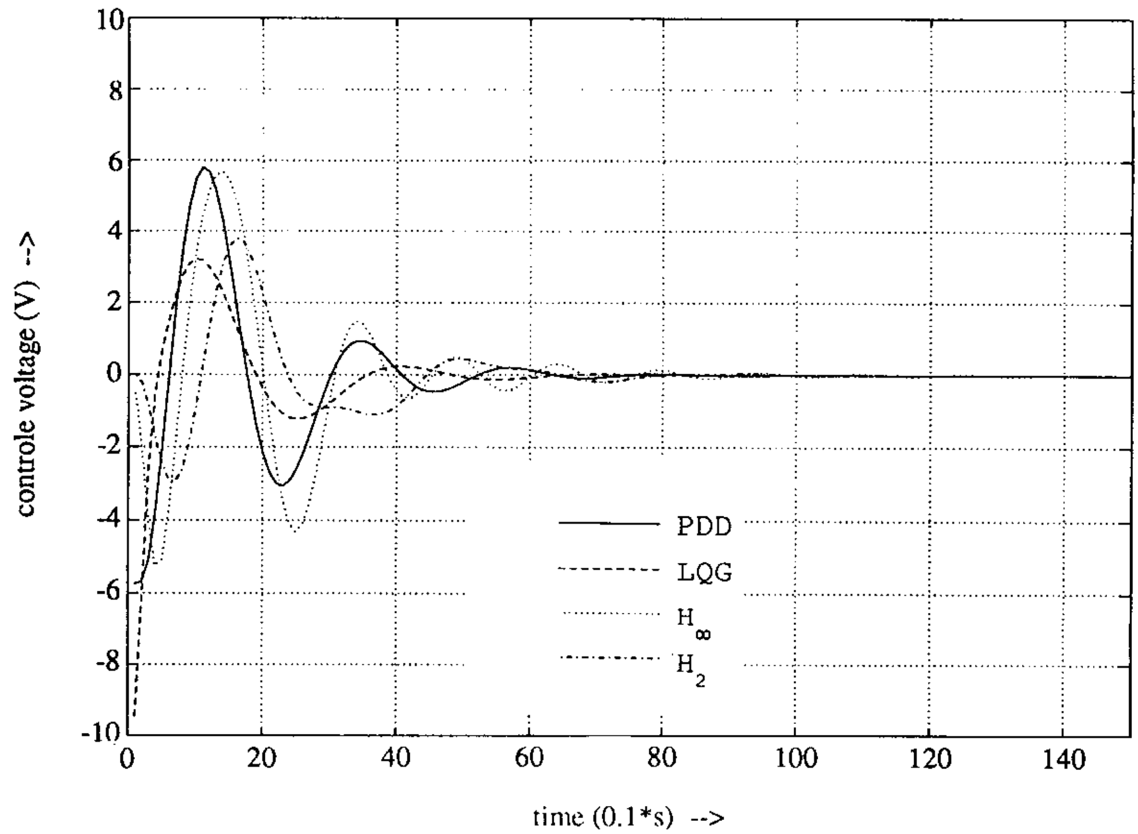

Fig. 6.2b, simulated control voltages of all four controllers.

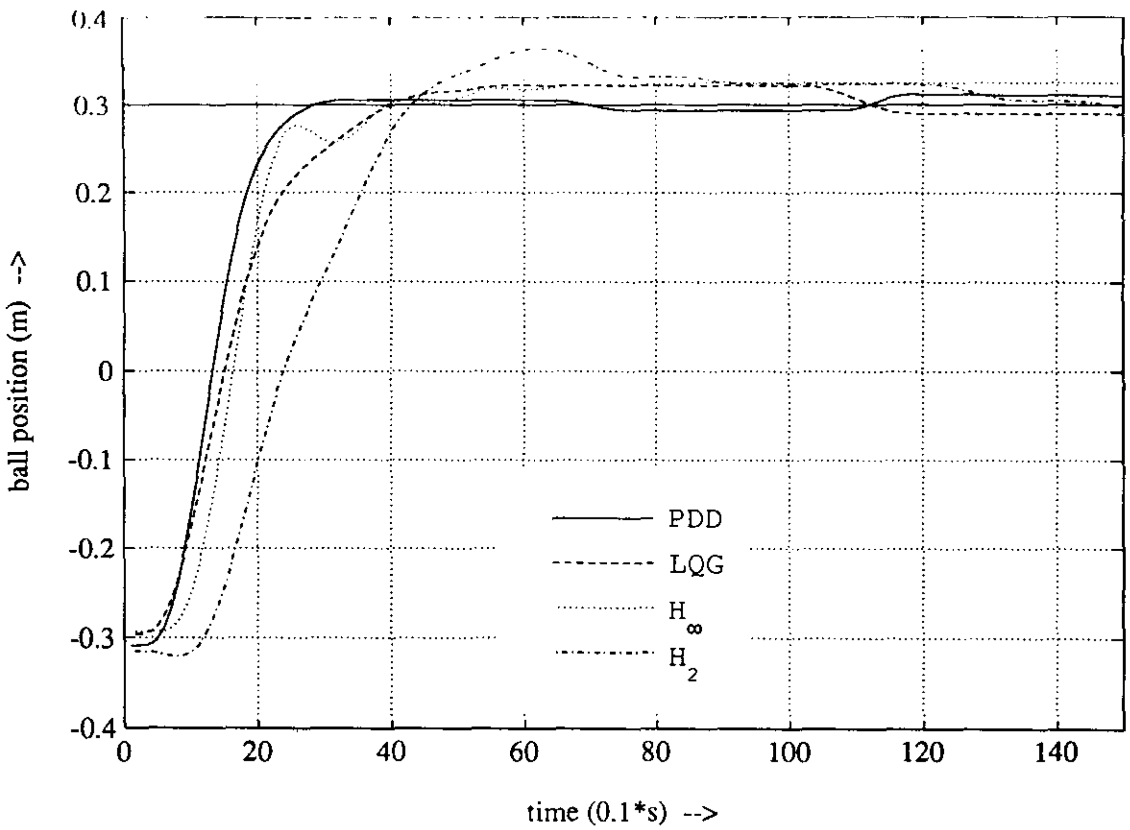

Fig. 6.2c, measured step responses of all four controllers.

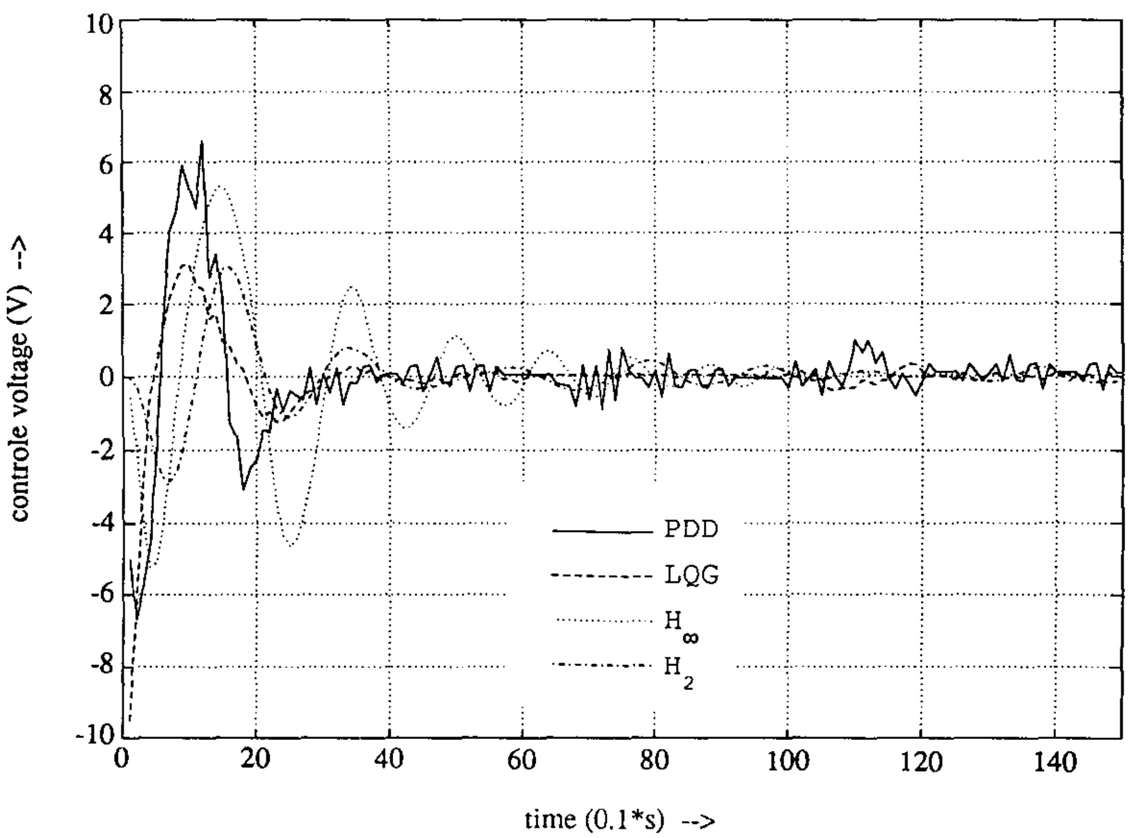

Fig. 6.2d, measured control voltages of all four controllers.

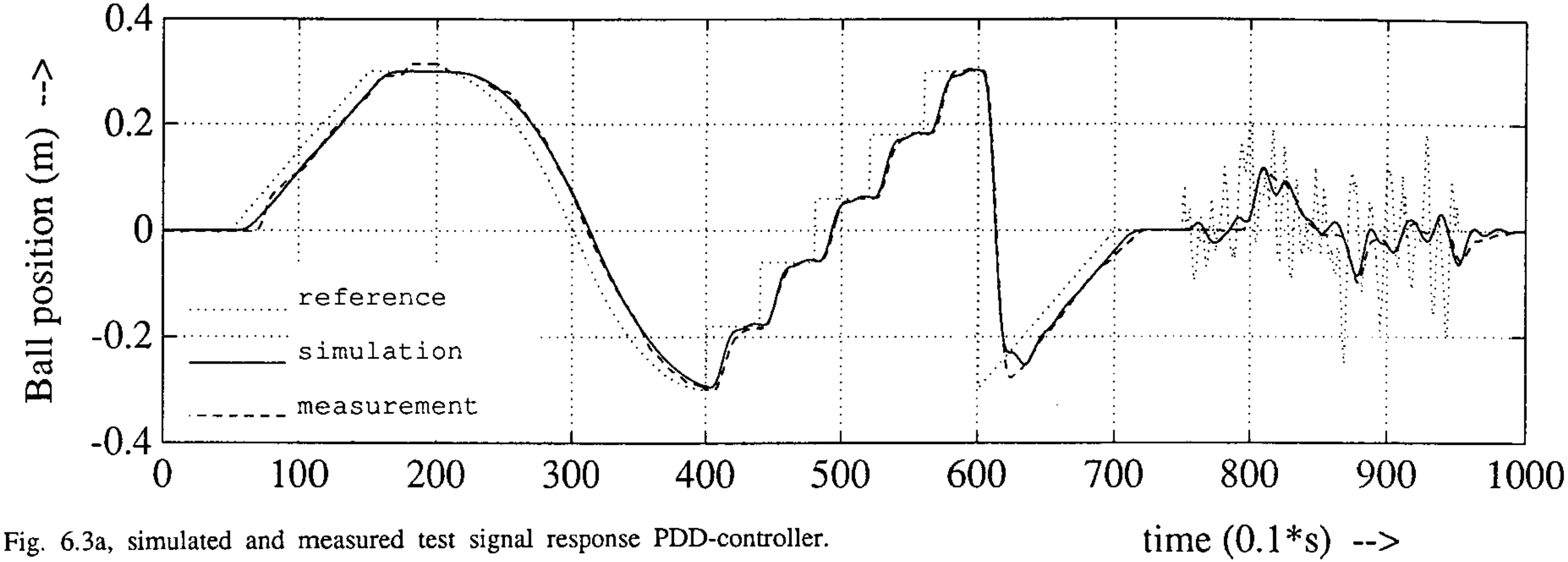

Fig. 6.3a, simulated and measured test signal response PDD-controller.

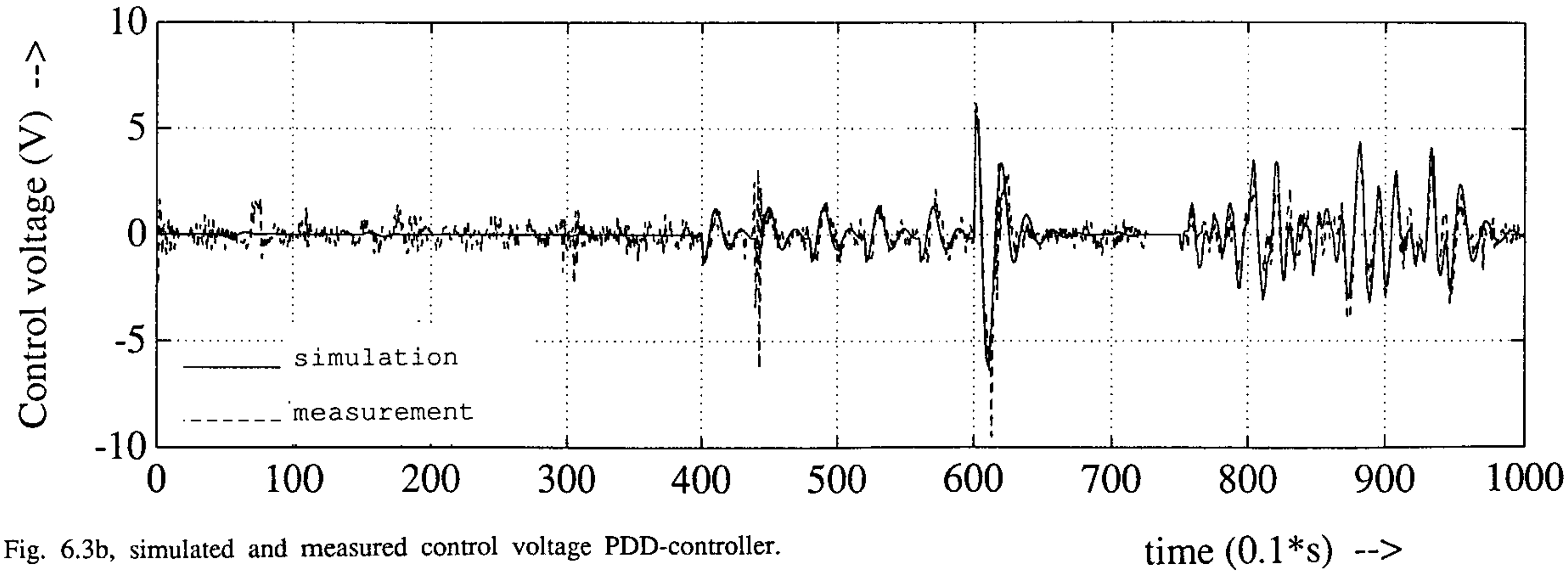

Fig. 6.3b, simulated and measured control voltage PDD-controller.

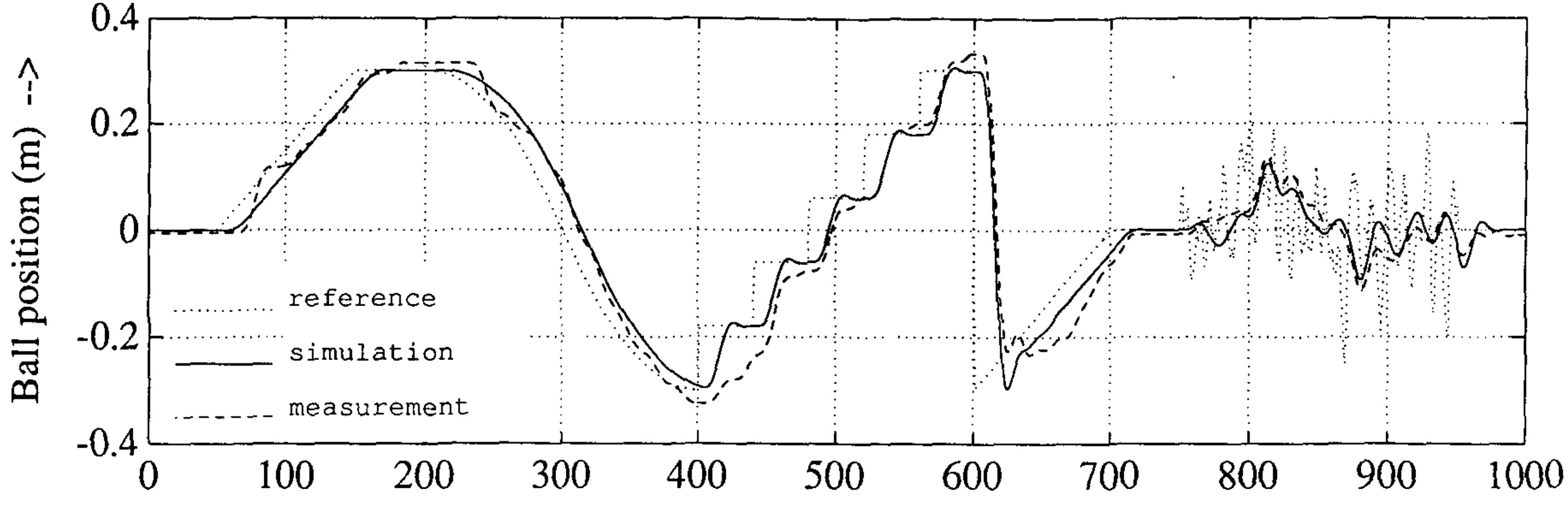

Fig. 6.3c, simulated and measured test signal response LQG-controller.

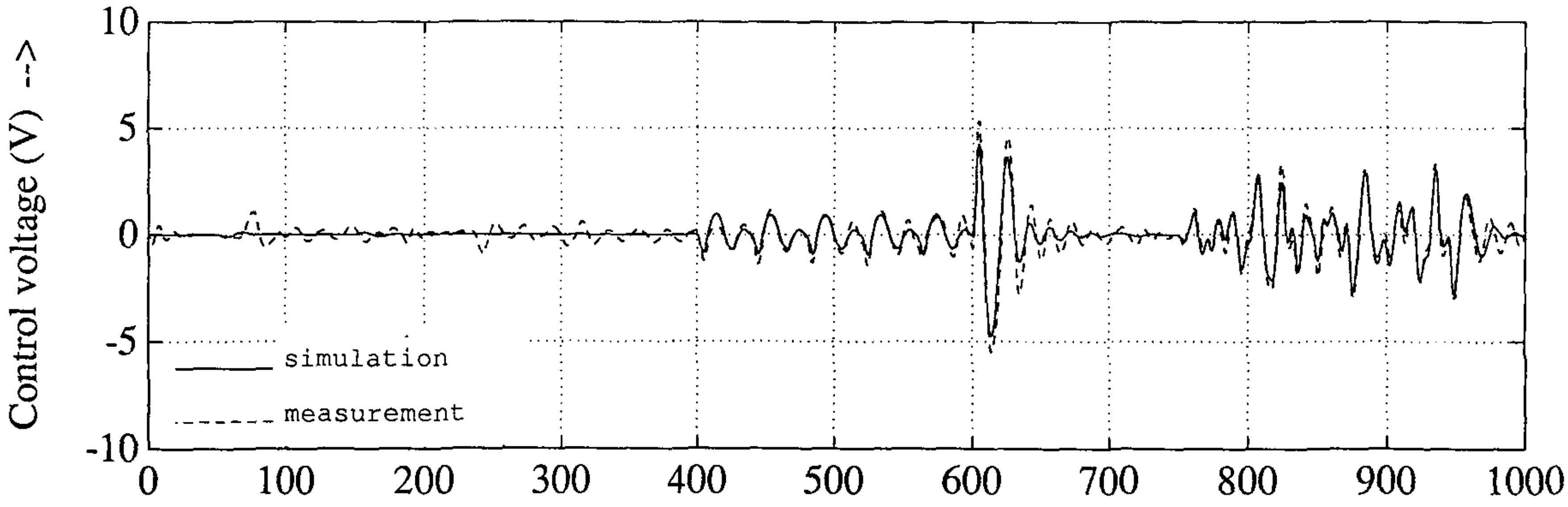

Fig. 6.3d, simulated and measured control voltage LQG-controller.

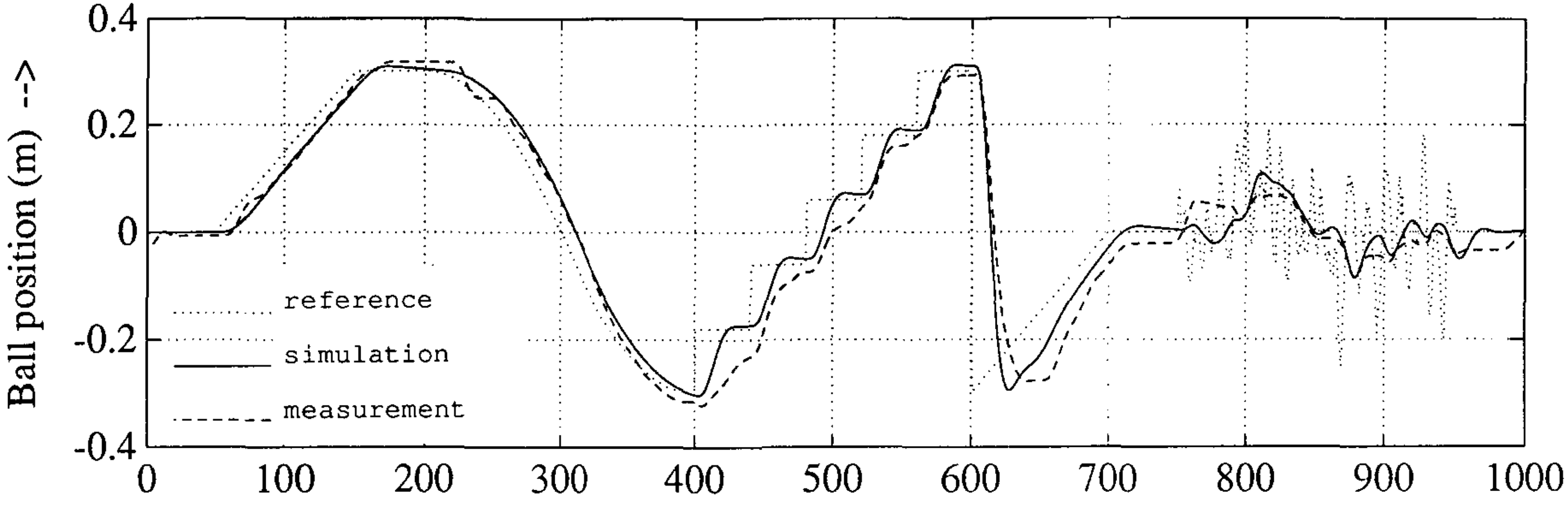

Fig. 6.3e, simulated and measured test signal response H_∞-controller.

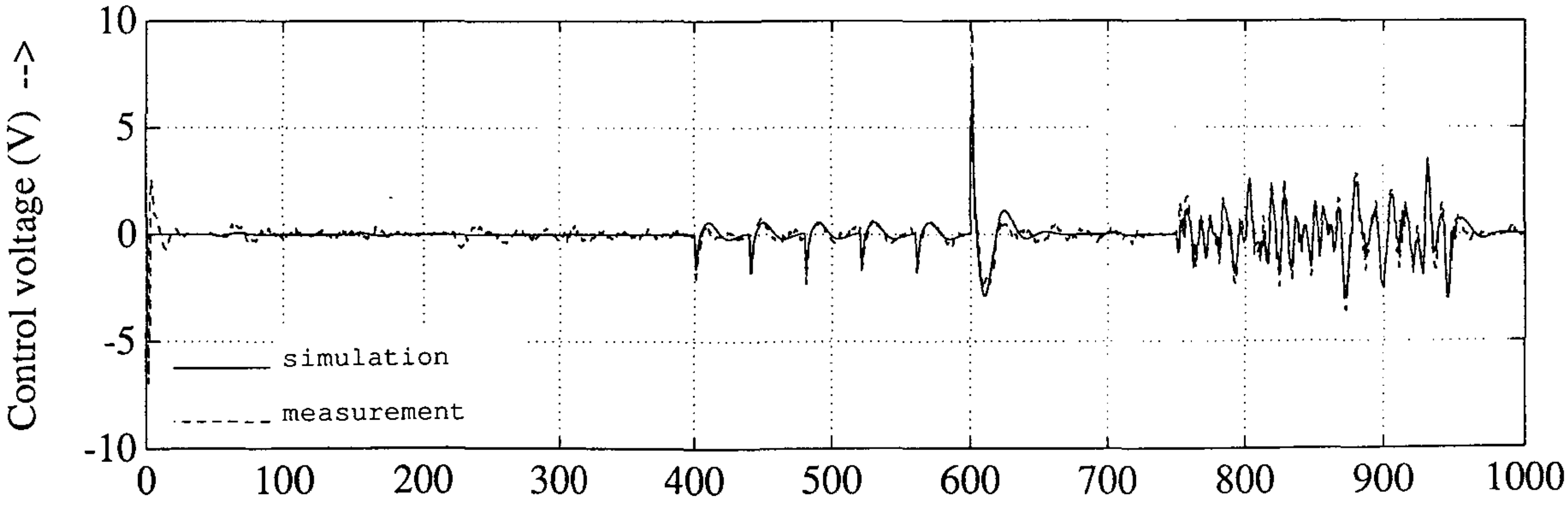

Fig. 6.3f, simulated and measured control voltage H_∞-controller.

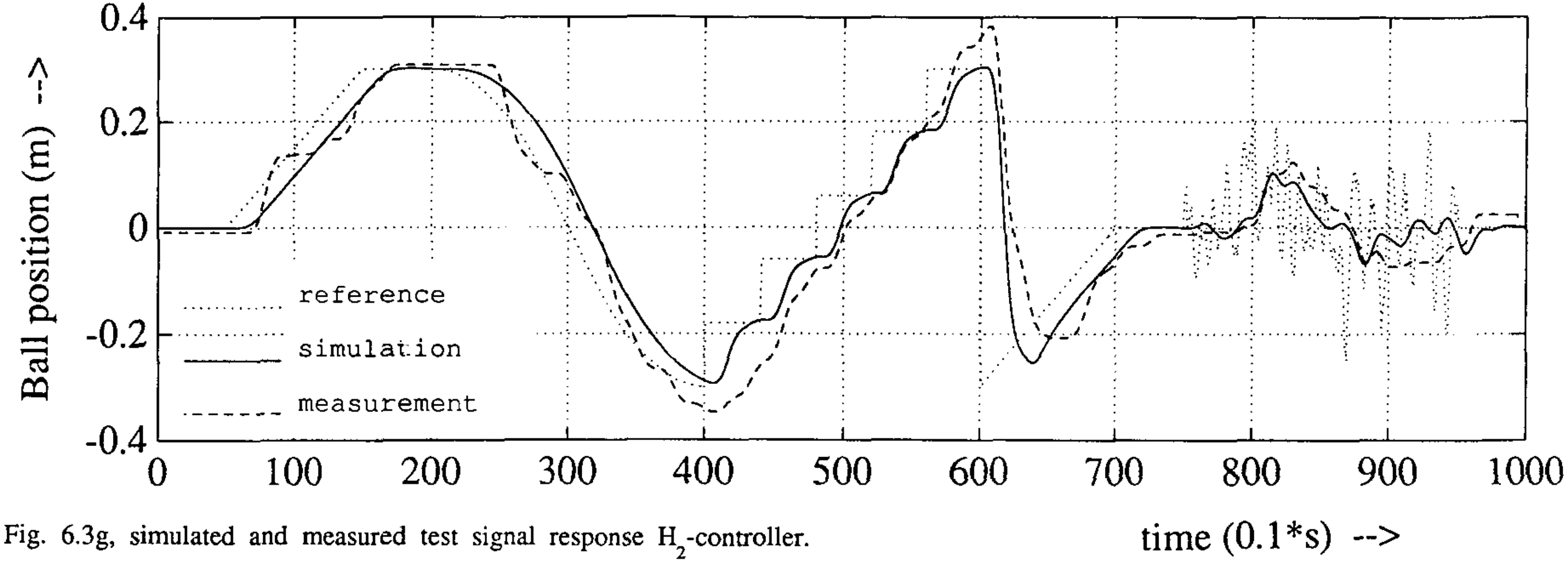

Fig. 6.3g, simulated and measured test signal response H_2-controller.

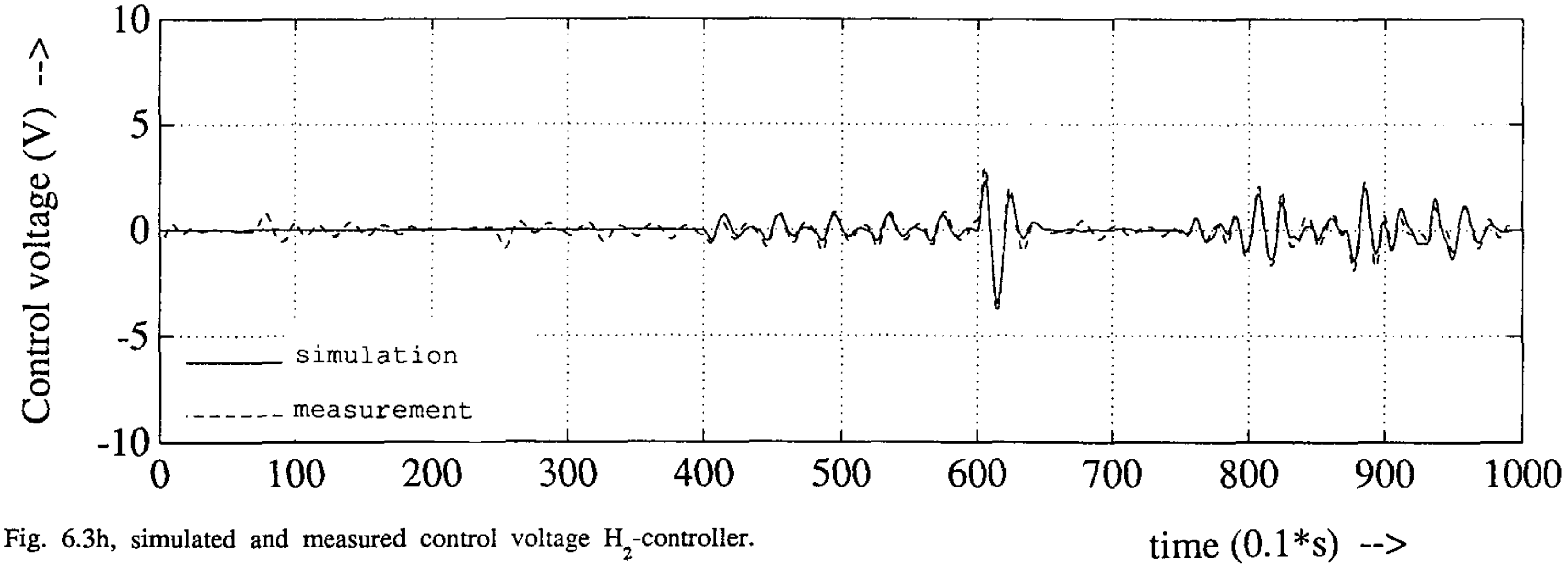

Fig. 6.3h, simulated and measured control voltage H_2-controller.

7. Comparison in the frequency domain

In the frequency domain the four controllers can be compared by considering:

- Signal tracking error (amplitude Bode plot): $E(z) = (y - r) / r$ (see Fig. 6.4).
- Power transfer function (amplitude Bode plot): $F(z) = u / r$ (see Fig. 6.5).
- Largest singular value of the weighted mixed-sensitivity-matrix:

$$\bar{\sigma}\{\mathcal{M}_2(z)\} = \bar{\sigma}\left(\begin{bmatrix} W_e(I - K_2P)^{-1}V_v \\ W_uK_2(I - K_2P)^{-1}V_v \end{bmatrix}\right) \quad \text{(see Fig. 6.6).}$$

- The H_∞ and H_2-norm of the criterion $\mathcal{M}(z)$ (see Table 6.2).
- The H_∞-norm of the weighted mixed-sensitivity-matrix and the corresponding robustness margin ε (see Table 6.3).
- Nyquist-diagrams and rootloci (see Figs. 6.7 to 6.8d-2 and Table 6.4).

From Fig. 6.4 & 6.5 follows that the PDD, LQG and H_∞-controller perform well as the band of good tracking is concerned. However, The PDD and the H_∞-controller show large peaks in the power transfer function, which can easily lead to saturation, the LQG and the H_2-controller perform better in saturation matters.

From Fig. 6.6: The H_∞-controller yields the best robustness as expected, but the H_2-controller comes very close, while the PDD-controller is very robust in the range from 10^{-3} till 10^{0}.

Table 6.2 shows the values for the H_∞ and H_2-norm of the criterion $\mathcal{M}(z)$ for all controllers (using the weighting functions as defined in Section 5). The H_2-norm of $\mathcal{M}(z)$ is calculated by means of a state-space realization of $\mathcal{M}(z)$ i.e. $\|\mathcal{M}(z)\|_2 = [\mathrm{trace}(CPC^* + DD^*)]^{1/2}$ (see the appendix for a proof) where P is the (discrete) controllability gramian.

	$\|\mathcal{M}(z)\|_\infty$	$\|\mathcal{M}(z)\|_2$
PDD	8821	2063
LQG	1990	470.7
H_∞	15.0	7.32
H_2	20.6	6.39

Table 6.2, H_∞ and H_2-norm of criterion $\mathcal{M}(z)$.

Notice the tremendous differences in Table 6.2, which are in real contrast with the moderate deviations between the various controller performances.

In Table 6.3 we give the values for $\|\mathcal{M}_2(z)\|_\infty$ and the resulting robustness margin ε (compare 5.4) for all controllers (using the weighting functions as defined in Section 5).

	$\|\mathcal{M}_2(z)\|_\infty$	ε
PDD	8796	$1.14 \cdot 10^{-4}$
LQG	1555	$6.43 \cdot 10^{-4}$
H_∞	10.0	0.100
H_2	13.5	0.0741

Table 6.3, H_∞-norm of the weighted-mixed-sensitivity matrix and robustness margin.

Certainly the H_∞-controller is most robust and we could expect a very bad robustness for the PDD and the LQG-controller, which is contradicted by the next traditional criteria of Nyquist and rootloci.

In Fig. 6.7 the Nyquist diagrams are given for all four controllers. For every controller this yields a fase margin and two gain margins (thus increasing or decreasing the gain will finally lead to instability) as given in Table 6.4.

	Gain margin 1 (in dB)	Gain margin 2 (in dB)	Fase margin (in degrees)
PDD	-8.68	+6.91	15.22
LQG	-12.82	+6.12	21.78
H_∞	-11.24	+3.56	18.82
H_2	-10.41	+3.52	22.52

Table 6.4, gain margins and fase margins.

In Fig. 6.8a-1 to 6.8d-2 the rootloci are given for the all four controllers where the gain γ of the feedback controller γK_2 is varied, $\gamma \geq 0$. The found "optimal" closed loop poles for each controller ($\gamma = 1$) are indicated by a "+". Particularly the simplicity of the PDD-controller attracts attention.

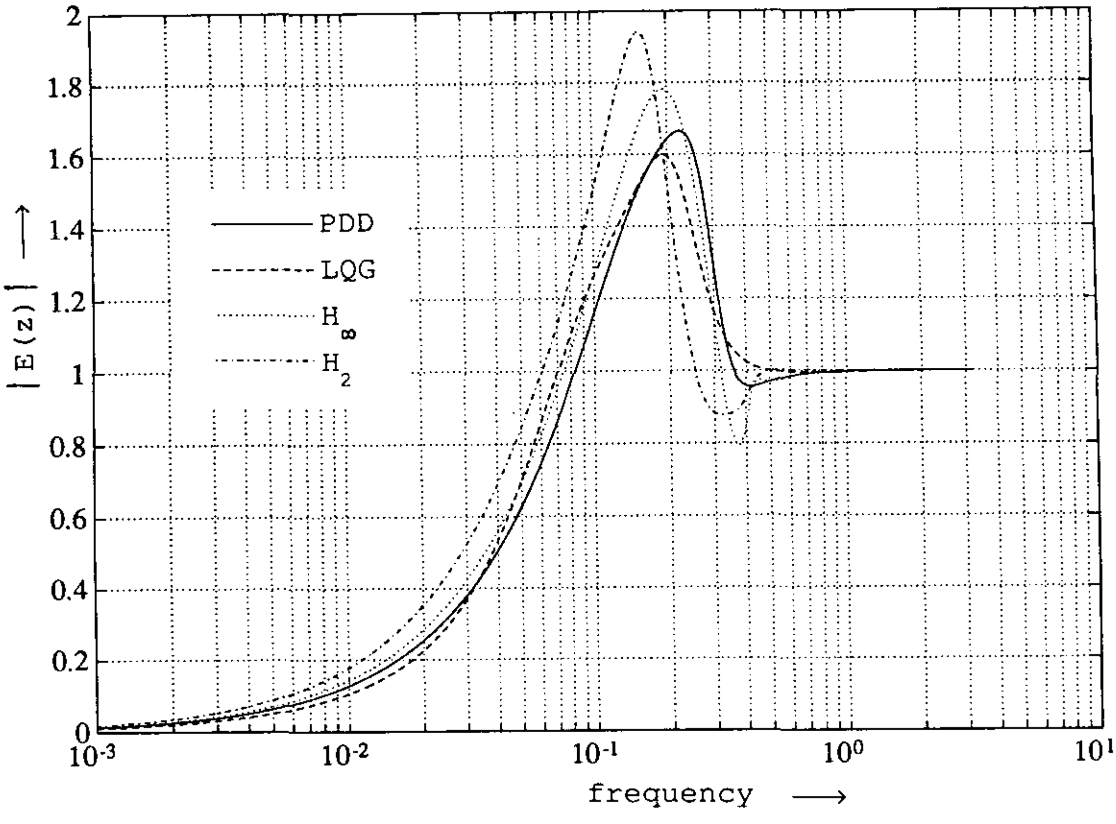

Fig. 6.4, Bode plot signal tracking error E(z).

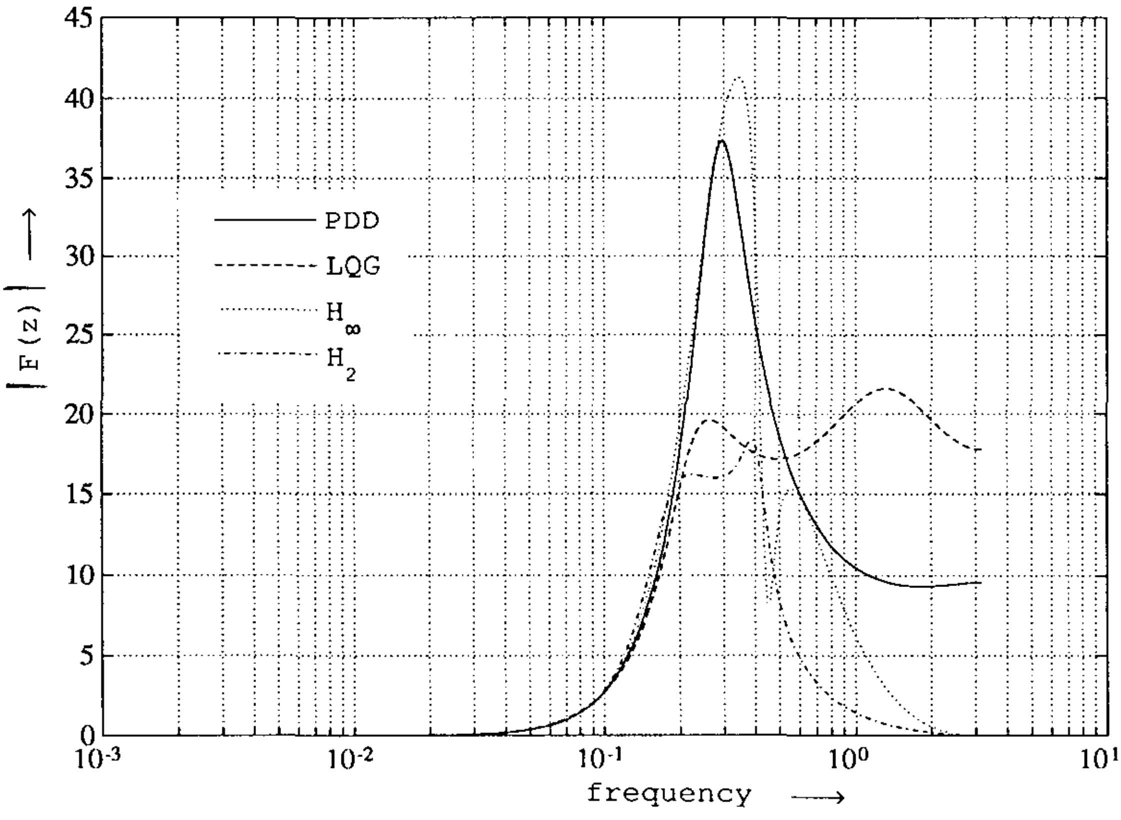

Fig. 6.5, Bode plot power transfer function F(z).

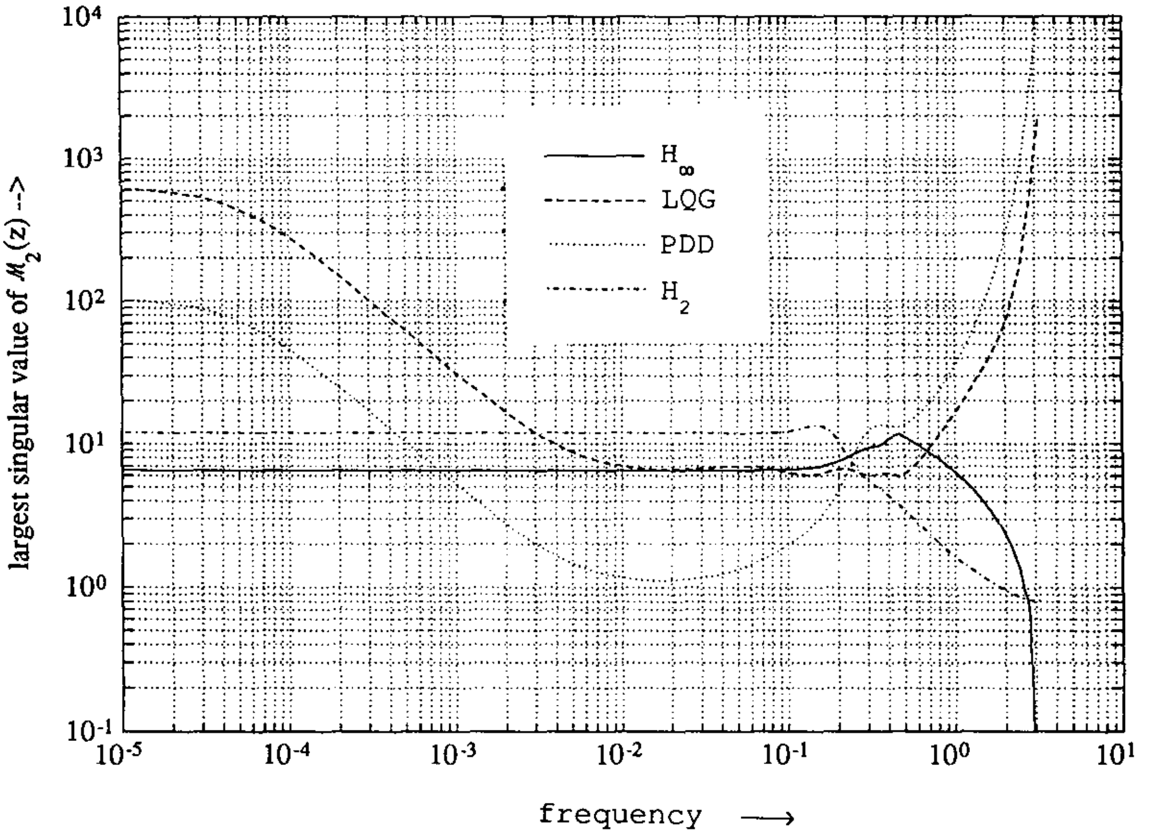

Fig. 6.6, largest singular value of $\mathcal{M}_2(z)$.

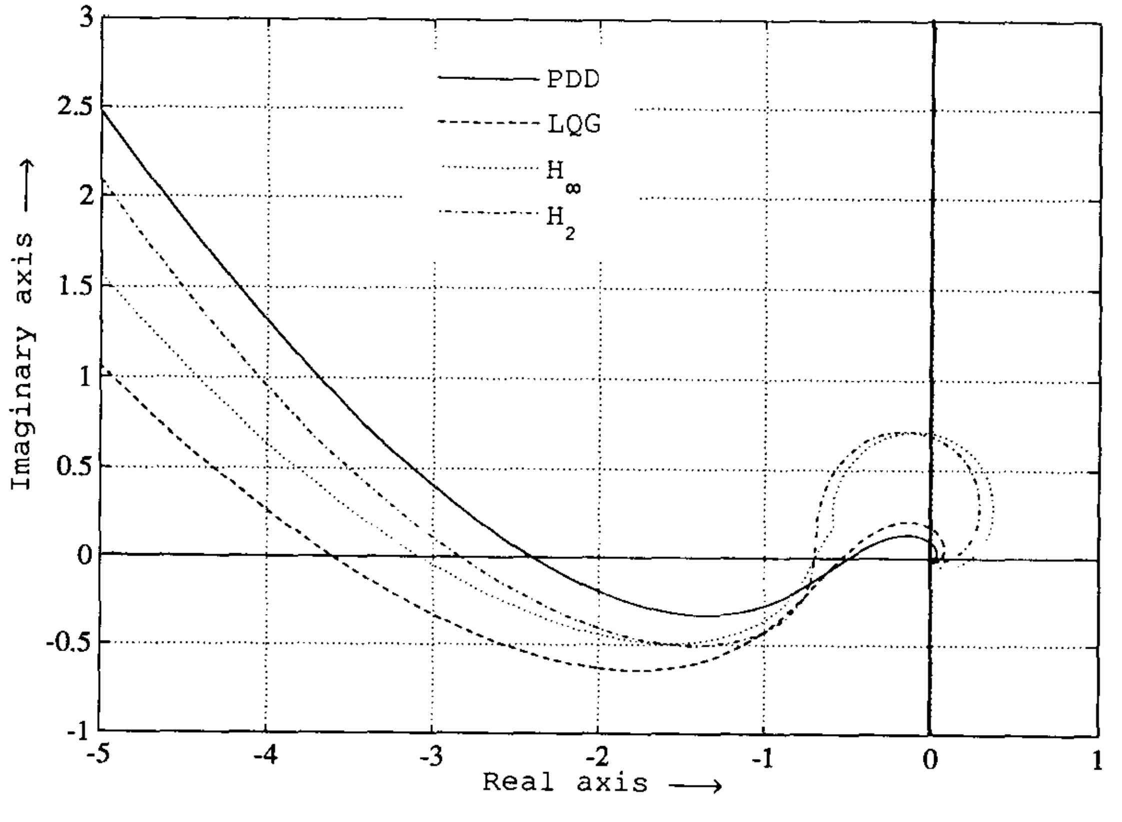

Fig. 6.7, Nyquist diagram of the four controllers.

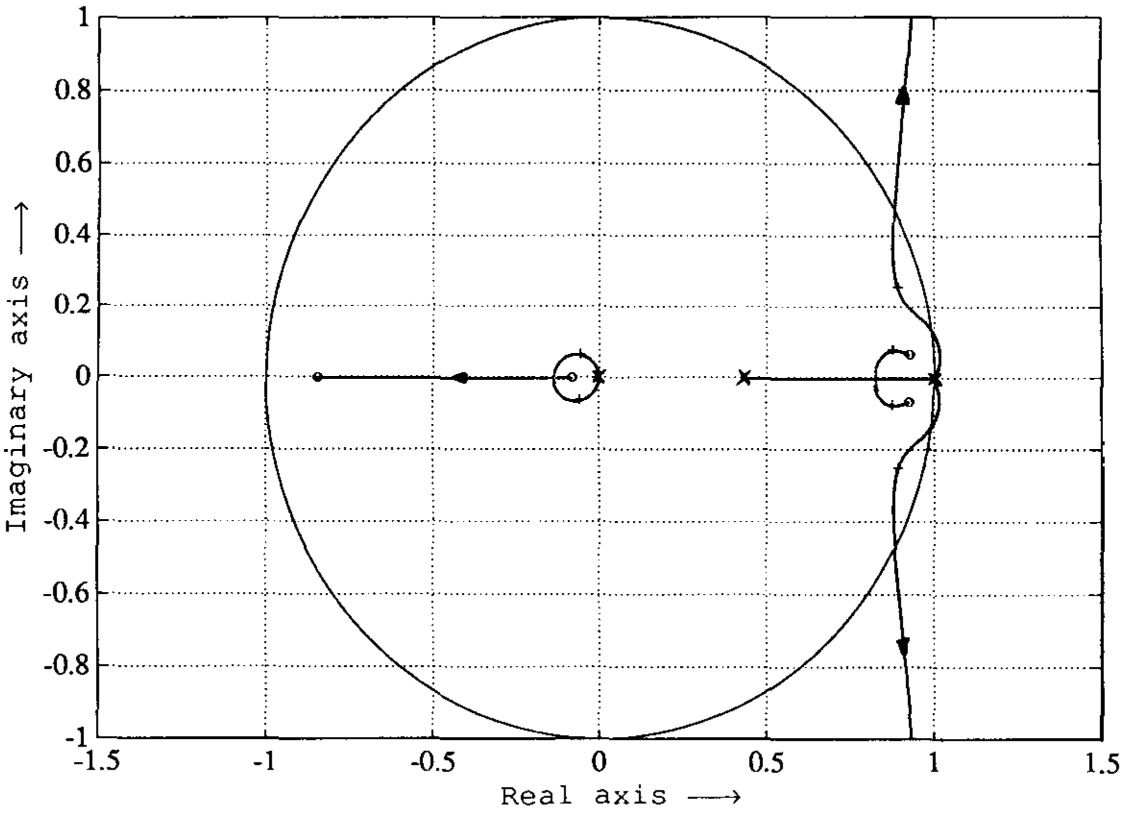

Fig. 6.8a-1, rootlocus of the PDD-controller.

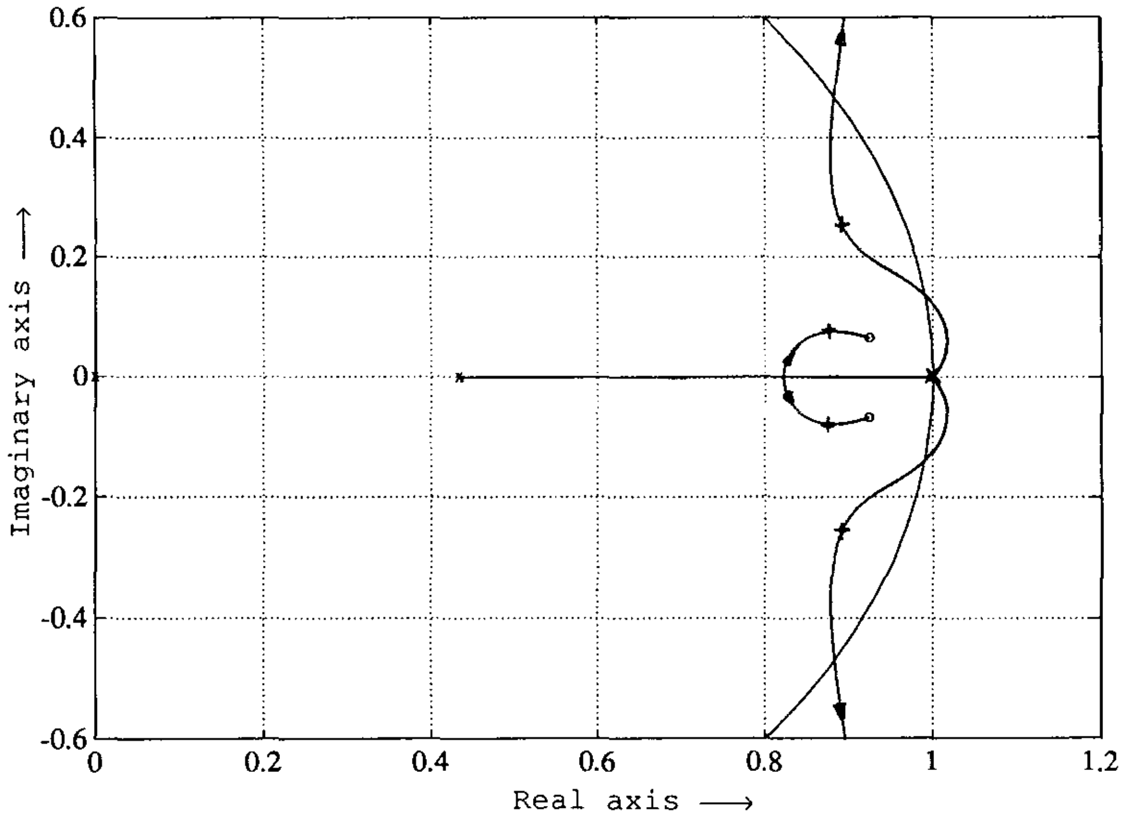

Fig. 6.8a-2, close-up rootlocus of the PDD-controller.

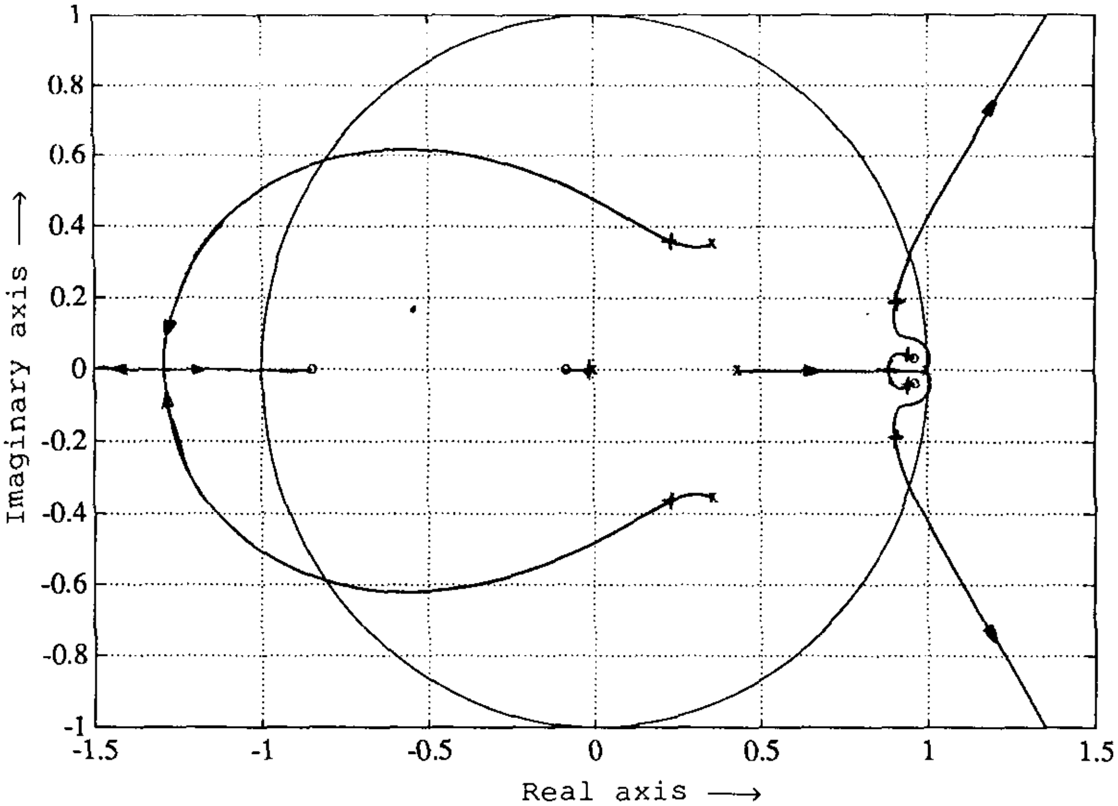

Fig. 6.8b-1, rootlocus of the LQG-controller.

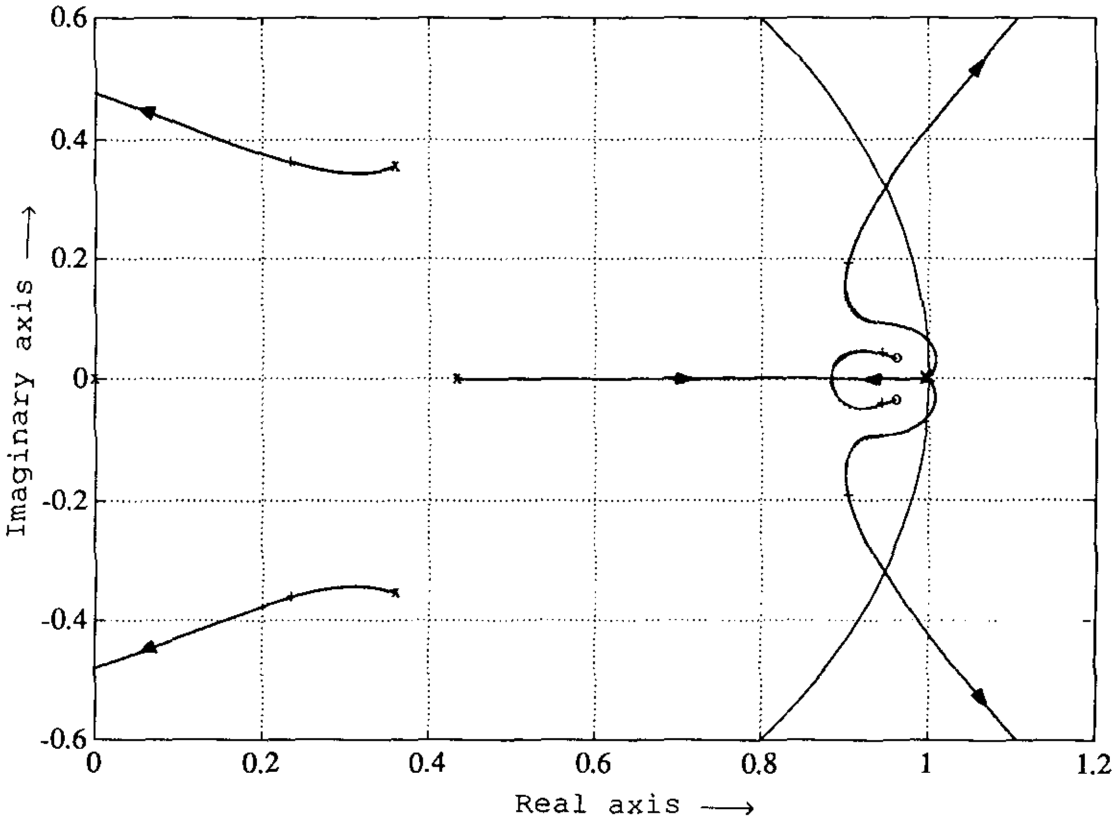

Fig. 6.8b-2, close-up rootlocus of the LQG-controller.

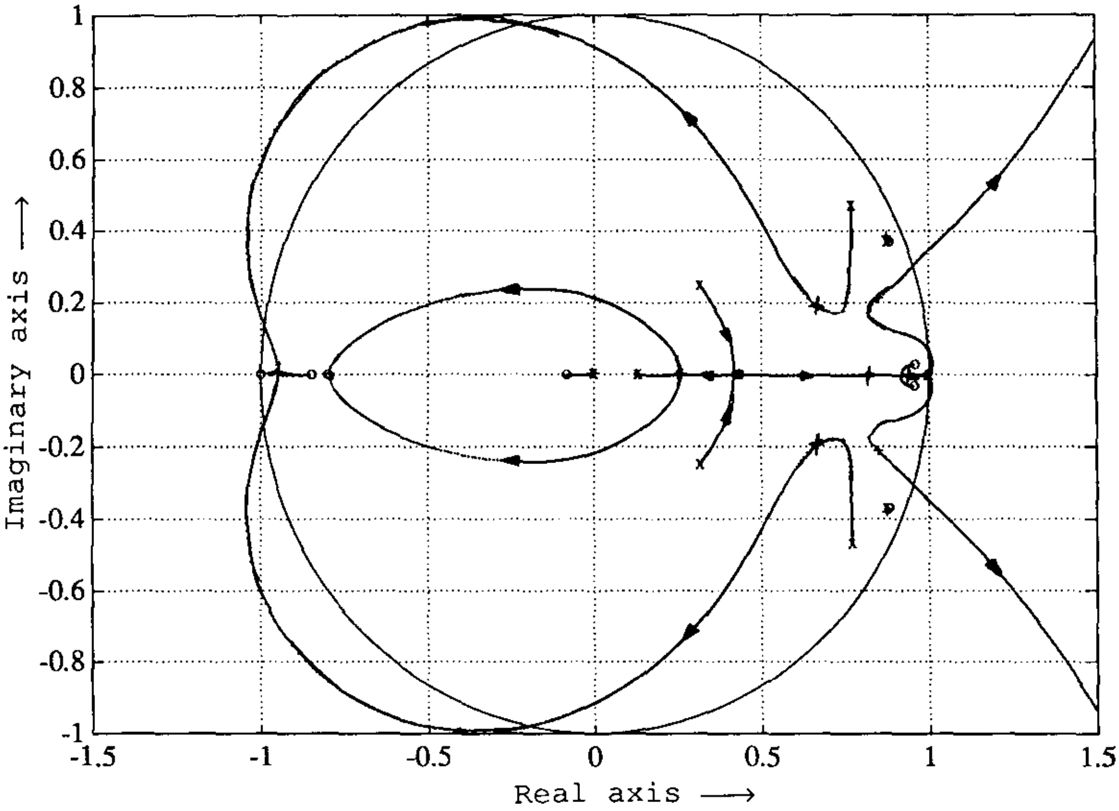

Fig. 6.8c-1, rootlocus of the H_∞-controller.

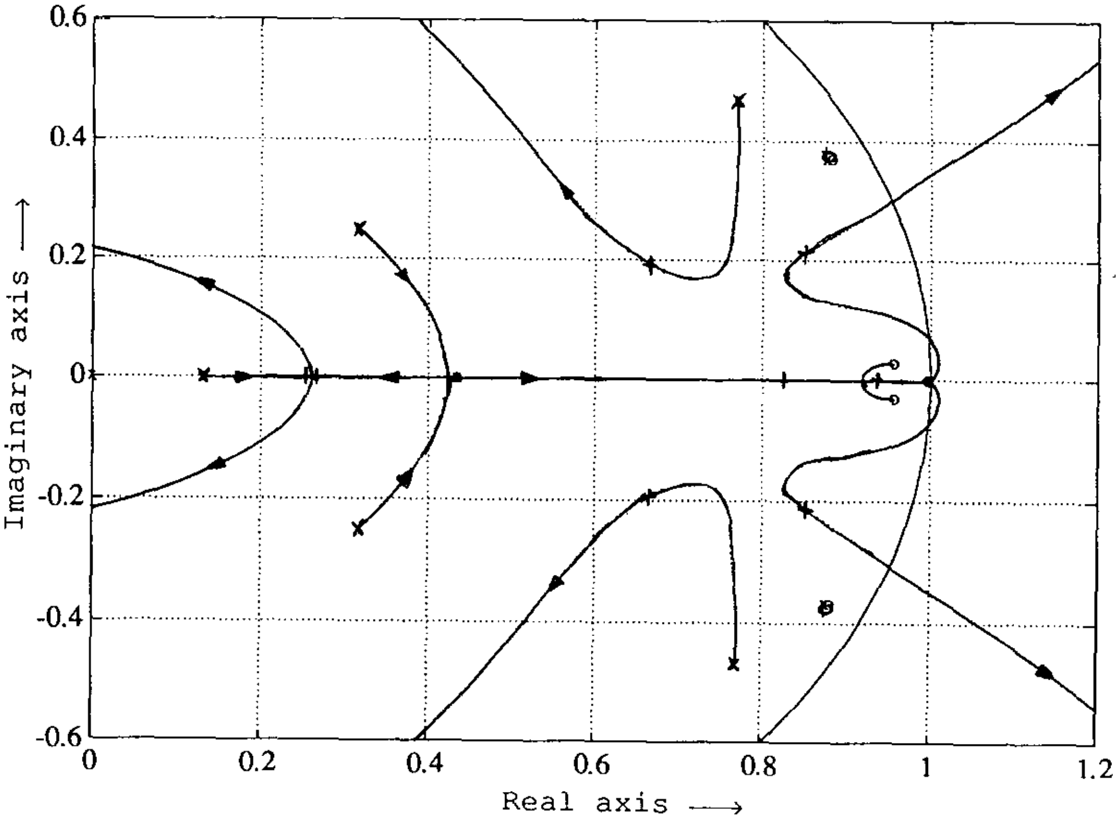

Fig. 6.8c-2, close-up rootlocus of the H_∞-controller.

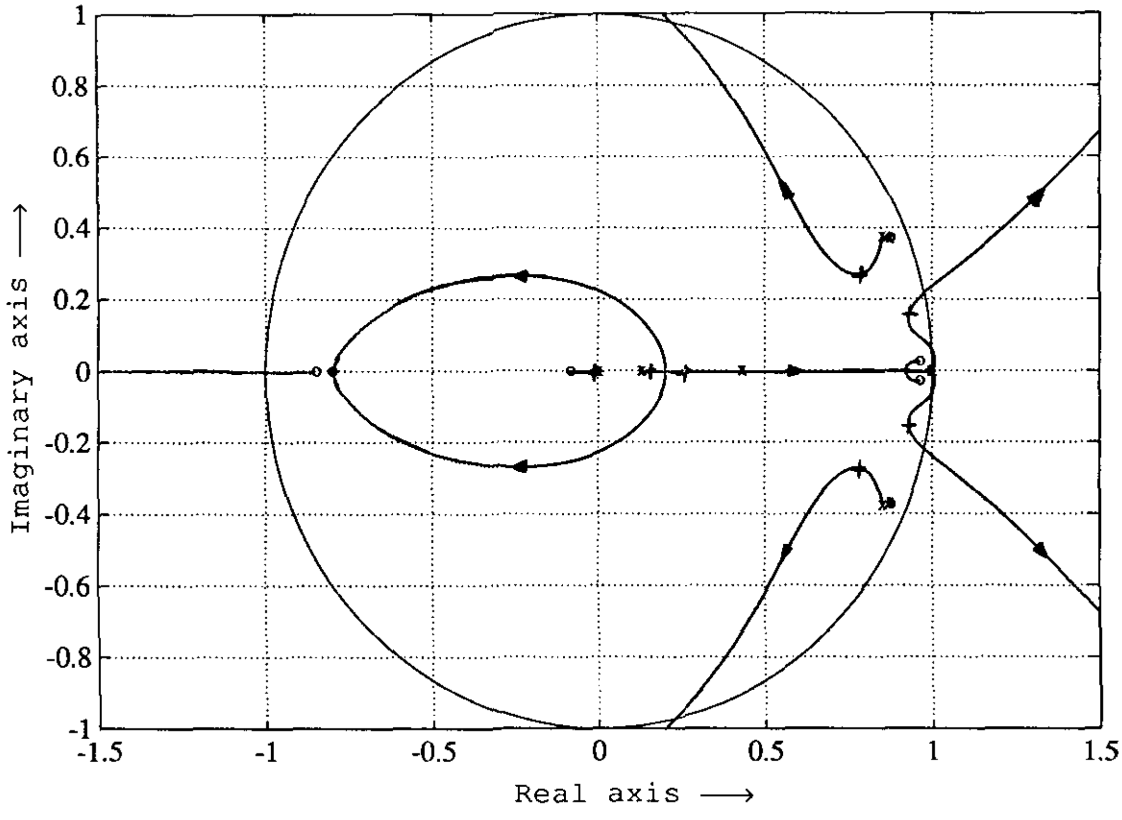

Fig. 6.8d-1, rootlocus of the H_2-controller.

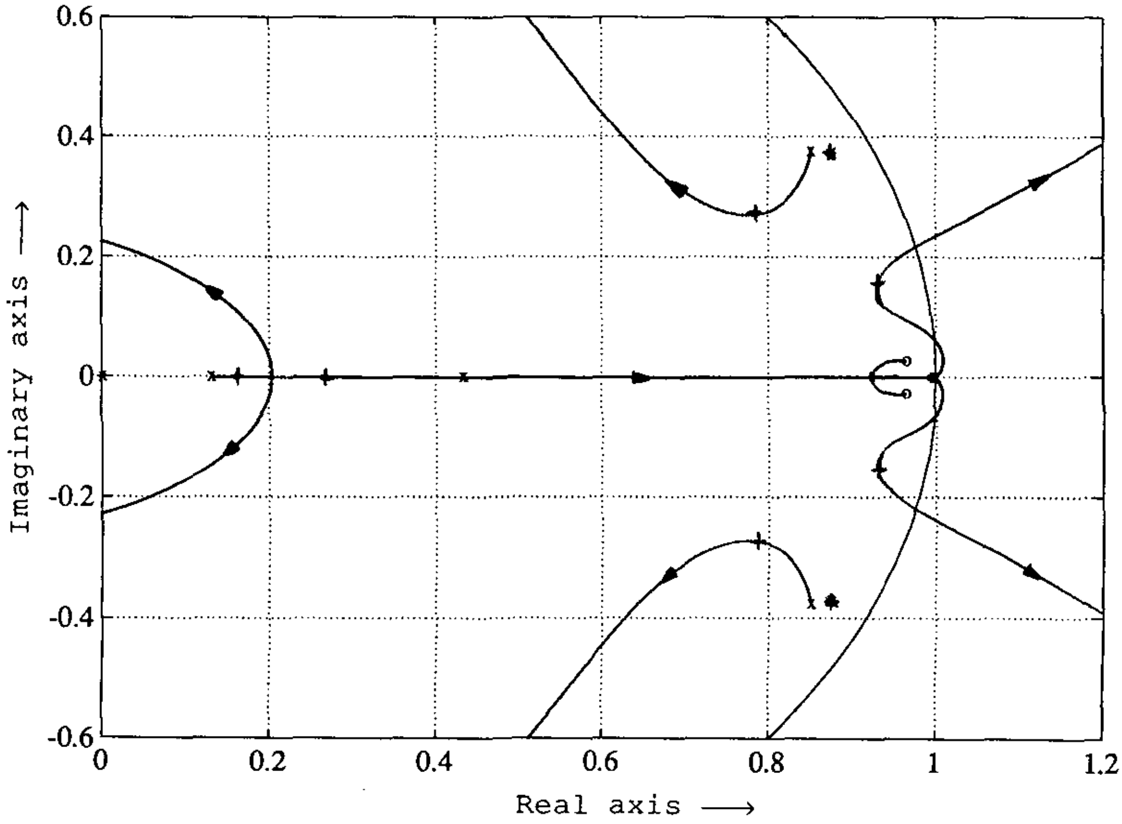

Fig. 6.8d-2, close-up rootlocus of the H_2-controller.

8. Discussion and conclusions

First some remarks about the various design methods. The design of the PDD-controller is without doubt the most simple one, it is based on classical tools like rootloci, Bode plots and only an approximate model is needed. The performance of the obtained controller is quite good considering the response to a step of 0.6 and the response to the special test signal plotted in Fig. 6.1a & 6.3a, also the tracking band width observed in Fig. 6.4 is very good. The PDD-controller has the worst robustness margin ε compared to the other controllers, see Table 6.3. On the other hand, the performance robustness is sufficient, see Fig. 6.1a & 6.1b.

The design of the LQG-controller is essentially done in the time-domain and an accurate model and knowledge of the noise is required. The performance of the LQG-controller is theoretically comparable with the other controllers, see Fig. 6.2a, but the performance in practice is substantially worse, see Fig. 6.1c & 6.3c. Possibly this is due to less energetic control signals, used by the LQG-controller (and the H_2-controller), compared to the H_∞ and PDD-controllers, see Table 6.1. Besides, for the design of the LQG-controller a third order model is used, while all other designs were based upon a physical fourth order model. The LQG-controller also has a bad robustness margin ε compared to the H_∞ and H_2-controllers, see Table 6.3, but traditional stability robustness criteria do not confirm a possible worse robustness, see Fig. 6.7 and Table 6.4.

The H_∞-controller design is done in the frequency-domain, using weighting filters to specify the control aims. Therefore frequency-demands are easily described but time-demands (like saturation) are difficult to catch. The performance of the H_∞-controller is comparable with the PDD-controller, though somewhat tardier, see Fig. 6.2a. The H_∞-controller is the most robust controller according to Table 6.3. The main problem of the H_∞-design method is its complexity and also the freedom in the choice of the weighting filters is difficult to handle.

Finally the H_2-controller; in principle the same remarks holds for the design of the H_2-controller as for the H_∞-controller. Only the resultant performance shows a substantially retarded response, see Fig. 6.1g, 6.2c & 6.3g this can also be observed in Fig. 6.5 where the H_2-controller has the smallest transfer from r to u for all frequencies. The H_2-controller also has the smallest tracking band width, see Fig. 6.4. An appropriate choice of weighting filters would be better, but finally lead to LQG-design.

Resuming the various topics:

- All design methods were greatly influenced by the design-constraint that no saturation is allowed when the input signal is a step of 0.6. In the PDD-design this constraint was handled simple by trial and error (simulations). In the LQG-design it is done by varying the R-matrix and in the H_∞/H_2-design by adjusting the weighting filter W_u. Fig. 6.5 shows that all controllers satisfy this design-constraint. The PDD and the H_∞-controller have a peak at 0.3 rad (≈ 0.5 Hz), but this peak has no influence when a step function is applied to the system.

- For the robustness stable-factor perturbations are considered instead of additive or multiplicative perturbations, because our nominal plant has three poles in $z = 1$. The physical interpretation of perturbations of the coprime factors is rather complex. The reason for this is that the coprime factorizations of the nominal plant can be done in many ways. To each factorization belongs a class of perturbed systems which are robustly stabilized by the controller to be designed. It is not clear how a factorization can be chosen that optimally corresponds to the expected modelling errors and process perturbations.

- The process under study is a SISO-process, so the design of controllers in the PID-class is easily done. However, if a MIMO-process is studied, and the model of the process is not accurate enough for a LQG-design, then the H_∞ and H_2-design methods can still be used.

References

[1] M.H. Driessen,
"Realization of a mechanical experimental process for education" (in Dutch), M.Sc. thesis, Measurement and Control Group, Faculty of Electrical Engineering, Eindhoven University of Technology, The Netherlands, 1987.

[2] A.J.J. van den Boom,
"H_∞-control: an exploratory study," Faculty of Electrical Engineering, Eindhoven University of Technology, The Netherlands, 1988. EUT Report 88-E-211.

[3] Advances in Multivariable Control. Lecture notes,
ONR/Honeywell Workshop, Minneapolis, Minn., 8-10 October 1984.
Workshop Coordinators: J. Doyle and J. Wall.
Honeywell Systems and Research Center, Aerospace and Defense Group, P.O. Box 312, Minneapolis, Minnesota 55440, USA.

[4] B.A. Francis,
"A course in H_∞ control theory," Berlin: Springer, 1987. Lecture notes in control and information sciences, , vol. 88.

[5] D.C. McFarlane and K. Glover,
"Robust controller design using normalized coprime factor plant descriptions," Berlin: Springer, 1990. Lecture notes in control and information sciences, vol. 138.

[6] M. Vidyasagar and H. Kimura,
"Robust controllers for uncertain linear multivariable systems,"
Automatica, vol. 22, pp. 85-94, January 1986.

[7] S.-Y. Kung and D.W. Lin,
"Optimal Hankel-norm model reductions: Multivariable systems,"
IEEE Trans. Autom. Control, vol. AC-26, pp. 832-852, August 1981.

[8] Ton van den Boom, Martin Klompstra and Ad Damen,
"A comparison of PDD, LQG, H_∞ and H_2-controllers for a laboratory process," in: Proc. 9th IASTED Int. Symp. on Modelling, Identification and Control, Innsbruck, Austria, 18-21 February 1990. Ed. by M.H. Hamza. Anaheim, Cal.: Acta Press, 1990. pp. 130-133.

[9] P. van Bemmelen,
"Identification of the ball-balancing system, using non-linear models based on physical insight," M.Sc. thesis, Measurement and Control Group, Faculty of Electrical Engineering, Eindhoven University of Technology, The Netherlands, 1988.

[10] R. Hanus, M. Kinnaert and J.-L. Henrotte,
"Conditioning technique, a general anti-windup and bumpless transfer method," Automatica, vol. 23, pp. 729-739, November 1987.

[11] J.C. Doyle, K. Glover, P.P. Khargonekar and B.A. Francis,
"State-space solutions to standard H_2 and H_∞ control problems," IEEE Trans. Autom. Control, vol. AC-34, pp. 831-847, August 1989.

Appendix

Consider the linear time-invariant discrete time system:

$$\left.\begin{aligned} x(k+1) &= Ax(k) + Bu(k) \\ y(k) &= Cx(k) + Du(k) \end{aligned}\right\} \tag{A.1}$$

with $k \in \mathbb{N}$, A stable (i.e. all eigenvalues inside the unit circle), (A,B) controllable, (A,C) observable and $x(0) = 0$. The impulse response of system (A.1) is defined as:

$$h(k) = \begin{cases} D & \text{for } k = 0 \\ CA^{k-1}B & \text{for } k \geq 1 \end{cases}$$

The transfer matrix H(z) is the z-transform of the impulse response h(k). The H_2-norm of H(z) can be computed from its definition in the beginning of Section 5, but an alternative characterisation can be given by using Parseval's formula and the definition of the impulse response:

$$\|H(z)\|_2^2 = \|h(k)\|_2^2 = \sum_{k=0}^{\infty} \text{trace}(h(k)h^*(k)) = \text{trace}(DD^* + \sum_{k=1}^{\infty} CA^{k-1}BB^*(A^*)^{k-1}C^*) =$$

$$= \text{trace}(DD^* + C\left\{\sum_{k=0}^{\infty} A^kBB^*(A^*)^k\right\}C^*) = \text{trace}(DD^* + CPC^*)$$

where P denotes the controllability gramian and is the unique positive definite symmetric solution of the discrete Lyapunov equation:

$$P - APA^* = BB^*$$

Analogously:

$$\|H(z)\|_2^2 = \text{trace}(DD^* + B^*QB)$$

where Q denotes the observability gramian and is the unique positive definite symmetric solution of the discrete Lyapunov equation:

$$Q - A^*QA = C^*C$$

ISSN 0167-9708
Coden: TEUEDE

(222) Jóźwiak, L.
THE FULL-DECOMPOSITION OF SEQUENTIAL MACHINES WITH THE SEPARATE REALIZATION OF THE NEXT-STATE AND OUTPUT FUNCTIONS.
EUT Report 89-E-222. 1989. ISBN 90-6144-222-2

(223) Jóźwiak, L.
THE BIT FULL-DECOMPOSITION OF SEQUENTIAL MACHINES.
EUT Report 89-E-223. 1989. ISBN 90-6144-223-0

(224) Book of abstracts of the first Benelux-Japan Workshop on Information and Communication Theory, Eindhoven, The Netherlands, 3-5 September 1989.
Ed. by Han Vinck.
EUT Report 89-E-224. 1989. ISBN 90-6144-224-9

(225) Hoeijmakers, M.J.
A POSSIBILITY TO INCORPORATE SATURATION IN THE SIMPLE, GLOBAL MODEL OF A SYNCHRONOUS MACHINE WITH RECTIFIER.
EUT Report 89-E-225. 1989. ISBN 90-6144-225-7

(226) Dahiya, R.P. and E.M. van Veldhuizen, W.R. Rutgers, L.H.Th. Rietjens
EXPERIMENTS ON INITIAL BEHAVIOUR OF CORONA GENERATED WITH ELECTRICAL PULSES SUPERIMPOSED ON DC BIAS.
EUT Report 89-E-226. 1989. ISBN 90-6144-226-5

(227) Bastings, R.H.A.
TOWARD THE DEVELOPMENT OF AN INTELLIGENT ALARM SYSTEM IN ANESTHESIA.
EUT Report 89-E-227. 1989. ISBN 90-6144-227-3

(228) Hekker, J.J.
COMPUTER ANIMATED GRAPHICS AS A TEACHING TOOL FOR THE ANESTHESIA MACHINE SIMULATOR.
EUT Report 89-E-228. 1989. ISBN 90-6144-228-1

(229) Oostrom, J.H.M. van
INTELLIGENT ALARMS IN ANESTHESIA: An implementation.
EUT Report 89-E-229. 1989. ISBN 90-6144-229-X

(230) Winter, M.R.M.
DESIGN OF A UNIVERSAL PROTOCOL SUBSYSTEM ARCHITECTURE: Specification of functions and services.
EUT Report 89-E-230. 1989. ISBN 90-6144-230-3

(231) Schemmann, M.F.C. and H.C. Heyker, J.J.M. Kwaspen, Th.G. van de Roer
MOUNTING AND DC TO 18 GHz CHARACTERISATION OF DOUBLE BARRIER RESONANT TUNNELING DEVICES.
EUT Report 89-E-231. 1989. ISBN 90-6144-231-1

(232) Sarma, A.D. and M.H.A.J. Herben
DATA ACQUISITION AND SIGNAL PROCESSING/ANALYSIS OF SCINTILLATION EVENTS FOR THE OLYMPUS PROPAGATION EXPERIMENT.
EUT Report 89-E-232. 1989. ISBN 90-6144-232-X

(233) Nederstigt, J.A.
DESIGN AND IMPLEMENTATION OF A SECOND PROTOTYPE OF THE INTELLIGENT ALARM SYSTEM IN ANESTHESIA.
EUT Report 90-E-233. 1990. ISBN 90-6144-233-8

(234) Philippens, E.H.J.
DESIGNING DEBUGGING TOOLS FOR SIMPLEXYS EXPERT SYSTEMS.
EUT Report 90-E-234. 1990. ISBN 90-6144-234-6

(235) Heffels, J.J.M.
A PATIENT SIMULATOR FOR ANESTHESIA TRAINING: A mechanical lung model and a physiological software model.
EUT Report 90-E-235. 1990. ISBN 90-6144-235-4

(236) Lammers, J.O.
KNOWLEDGE BASED ADAPTIVE BLOOD PRESSURE CONTROL: A Simplexys expert system application.
EUT Report 90-E-236. 1990. ISBN 90-6144-236-2

(237) Ren Qingchang
PREDICTION ERROR METHOD FOR IDENTIFICATION OF A HEAT EXCHANGER.
EUT Report 90-E-237. 1990. ISBN 90-6144-237-0

ISSN 0167-9708
Coden: TEUEDE

(238) Lammers, J.O.
THE USE OF PETRI NET THEORY FOR SIMPLEXYS EXPERT SYSTEMS PROTOCOL CHECKING.
EUT Report 90-E-238. 1990. ISBN 90-6144-238-9

(239) Wang, X.
PRELIMINARY INVESTIGATIONS ON TACTILE PERCEPTION OF GRAPHICAL PATTERNS.
EUT Report 90-E-239. 1990. ISBN 90-6144-239-7

(240) Lutgens, J.M.A.
KNOWLEDGE BASE CORRECTNESS CHECKING FOR SIMPLEXYS EXPERT SYSTEMS.
EUT Eeport 90-E-240. 1990. ISBN 90-6144-240-0

(241) Brinker, A.C. den
A MEMBRANE MODEL FOR SPATIOTEMPORAL COUPLING.
EUT Report 90-E-241. 1990. ISBN 90-6144-241-9

(242) Demarteau, J.I.M. and H.C. Heyker, J.J.M. Kwaspen, Th.G. van de Roer
MICROWAVE NOISE FIGURE MEASUREMENTS ON DOUBLE BARRIER RESONANT TUNNELING DIODES.
EUT Report 90-E-242. 1990. ISBN 90-6144-242-7

(243) Massee, P. and H.A.L.M. de Graaf, W.J.M. Balemans, H.G. Knoopers, H.H.J. ten Kate
PREDESIGN OF AN EXPERIMENTAL (5-10 MWt) DISK MHD FACILITY AND PROSPECTS OF COMMERCIAL (1000 MWt) MHD/STEAM SYSTEMS.
EUT Report 90-E-243. 1990. ISBN 90-6144-243-5

(244) Klompstra, Martin and Ton van den Boom, Ad Damen
A COMPARISON OF CLASSICAL AND MODERN CONTROLLER DESIGN: A case study.
EUT Report 90-E-244. 1990. ISBN 90-6144-244-3

(245) Berg, P.H.G. van de
ON THE ACCURACY OF RADIOWAVE PROPAGATION MEASUREMENTS: Olympus propagation experiment.
EUT Report 90-E-245. 1990. ISBN 90-6144-245-1